

# Inhibition of SHP-1 activity by PKC- $\theta$ regulates NK cell activation threshold and cytotoxicity

Aviad Ben-Shmuel<sup>†</sup>, Batel Sabag<sup>†</sup>, Abhishek Puthenveetil, Guy Biber, Moria Levy, Tammir Jubany, Fatima Awwad, Roshan Kumar Roy, Noah Joseph, Omri Matalon, Jessica Kivelevitz, Mira Barda-Saad\*

The Mina and Everard Goodman Faculty of Life Sciences, Bar-Ilan University, Ramat Gan, Israel

**Abstract** Natural killer (NK) cells play a crucial role in immunity, killing virally infected and cancerous cells. The balance of signals initiated upon engagement of activating and inhibitory NK receptors with cognate ligands determines killing or tolerance. Nevertheless, the molecular mechanisms regulating rapid NK cell discrimination between healthy and malignant cells in a heterogeneous tissue environment are incompletely understood. The SHP-1 tyrosine phosphatase is the central negative NK cell regulator that dephosphorylates key activating signaling proteins. Though the mechanism by which SHP-1 mediates NK cell inhibition has been partially elucidated, the pathways by which SHP-1 is itself regulated remain unclear. Here, we show that phosphorylation of SHP-1 in NK cells on the S591 residue by PKC- $\theta$  promotes the inhibited SHP-1 ‘folded’ state. Silencing PKC- $\theta$  maintains SHP-1 in the active conformation, reduces NK cell activation and cytotoxicity, and promotes tumor progression in vivo. This study reveals a molecular pathway that sustains the NK cell activation threshold through suppression of SHP-1 activity.

**\*For correspondence:**

Mira.Barda-Saad@biu.ac.il

<sup>†</sup>These authors contributed equally to this work

**Competing interest:** The authors declare that no competing interests exist.

**Funding:** See page 25

**Received:** 23 August 2021

**Preprinted:** 06 September 2021

**Accepted:** 23 February 2022

**Published:** 08 March 2022

**Reviewing Editor:** Stipan Jonjic, University of Rijeka, Croatia

© Copyright Ben-Shmuel et al. This article is distributed under the terms of the [Creative Commons Attribution License](https://creativecommons.org/licenses/by/4.0/), which permits unrestricted use and redistribution provided that the original author and source are credited.

## Editor's evaluation

The study by Dr. Barda-Saad and colleagues deals with natural killer (NK) cells activation that depends on a balance between stimulatory and inhibitory signals. Inhibition of NK cells results from the recruitment of the protein tyrosine phosphatase, SHP-1, which dephosphorylates vital signaling molecules and thus reverses NK cell activation. This study describes how PKC regulates the activity of SHP-1 in the early stages of activation and inhibition of NK cell synapses and, by doing so, regulates their adaptation to the microenvironment in which they act.

## Introduction

Natural killer (NK) cells are a class of lymphocytes that comprise a central component of the innate immune system. They patrol the body and kill virally transformed and cancerous cells. NK cell effector functions are carried out by the release of cytotoxic granules containing perforin and Granzyme B, which induce target cell death (*Pipkin and Lieberman, 2007; Topham and Hewitt, 2009*). Furthermore, NK cells produce cytokines and chemokines, such as IFN- $\gamma$ , which activate the adaptive immune response (*Malhotra and Shanker, 2011*).

Activation or inhibition of NK function was shown to depend on the balance between signals derived from activating and inhibitory receptors on the NK cell surface (*Lanier, 2005*). Various motifs on the cytoplasmic tails of these receptors were shown to induce distinct downstream signaling cascades. These include immunoreceptor tyrosine-based activation motifs (ITAMs) found on cytoplasmic tails of

the transmembrane adaptor proteins CD3 $\zeta$ , Fc $\epsilon$ R1 $\gamma$ , and DAP12, or the YINM motif on the DAP10 adaptor, which associates with the NKG2D receptor (**André et al., 2004**). Another group of motifs includes the immunoreceptor tyrosine-based switch motifs (ITSMs) on the CD244 receptor (**Vyas et al., 2002b; Lanier, 2003; Feng et al., 2005**). Though NK cell receptors are well characterized, the molecular mechanisms downstream to receptor ligation, and how these are integrated to achieve the appropriate activation state, are incompletely understood.

Inhibitory NK cell receptors express a separate target sequence for signal suppression, consisting of immunoreceptor tyrosine-based inhibition motifs (ITIMs) expressed on the cytoplasmic tails (**Long, 2008**). The key receptors facilitating NK inhibition recognize major histocompatibility class 1 (MHC-I) molecules expressed on the majority of cells in the body. These receptors include the killer cell immunoglobulin-like receptor (KIR) family in humans and primates, the Ly49 family in mice, and NKG2A/CD94 receptors expressed in both primates and mice (**Orr and Lanier, 2010**). NGK2A/CD94 were shown to have specificity for the human leukocyte antigen (HLA) isoform E (HLA-E), whereas the KIR family of inhibitory receptors was shown to associate with HLA-C and HLA-B (**Moretta et al., 1994; Wagtmann et al., 1995**). Engagement of these receptors with their cognate ligands and phosphorylation of their ITIM motifs recruits the Src-homology 2-domain (SH2)-containing protein tyrosine phosphatase (PTP), SHP-1. SHP-1 consequently dephosphorylates key proteins involved in the activating signaling pathway, thereby downregulating NK cell activation (**Stebbins et al., 2003; Matalon et al., 2016**). SHP-1 comprises a catalytic phosphatase domain near its C' terminus, two phosphotyrosine binding SH2 domains toward its N' terminus, and sites of tyrosine and serine phosphorylation at the end of its C'-terminal tail (**Lorenz, 2009**). In its autoinhibited closed state, the SHP-1 N' SH2 domain associates with the catalytic domain, blocking access to its substrates.

Binding of SHP-1 SH2 domains to phosphorylated tyrosine residues on the ITIM of the inhibitory receptors induces a conformational alteration in SHP-1. This releases it from the inhibited state and enables its catalytic activity, that is, dephosphorylation of key signaling molecules and inhibition of NK cell function (**Wang et al., 2011**). SHP-1 substrates in NK cells include the guanine nucleotide exchange factor (GEF), VAV1 (**Stebbins et al., 2003**), phospholipase C gamma 1/2 (PLC $\gamma$ 1/2), and linker for activation of T cells (LAT), recently identified by our group (**Matalon et al., 2016**).

Though SHP-1 function is critical for correct NK cell immune responses, the manner by which its catalytic activity is regulated remains unclear. Elucidating this mechanism is especially important since NK cells engage target cells expressing both activating and inhibitory receptors, and SHP-1 recruitment to ITIMs decreases the activity of NK cells toward potential targets, despite expression of activating ligands. Therefore, upregulation of ligands for inhibitory NK receptors that express ITIMs by cancer cells, such as HLA-E and PD-L1, may repress NK cell activity through SHP-1 recruitment and activity (**Carretero et al., 1998; Chemnitz et al., 2004**). Identifying the factors that regulate SHP-1 activity may lead to a better understanding of how NK cell activity is accurately and rapidly tuned in tissues containing both healthy and transformed cells. We recently revealed that actin retrograde flow (ARF) induces a physical conformational change in the SHP-1 molecule to facilitate its activity (**Matalon et al., 2018**). However, key questions remain unresolved. SHP-1 was shown to localize to the lytic NK cell immunological synapse (NKIS) (**Vyas et al., 2002a**), yet the mechanism by which its activity at the lytic synapse is regulated was not determined. Furthermore, it is not clear how termination of SHP-1 activity occurs after NK cells are successfully inhibited, thereby enabling NK cells to function in subsequent interactions with activating target cells.

Thus, since SHP-1 is a critical checkpoint molecule in NK cells and regulates the NK cell activation threshold, it is of great interest to understand the underlying mechanisms that control its catalytic activity during the NK cell response.

Here, we demonstrate that in NK cells SHP-1 is heavily phosphorylated on the serine 591 residue (S591) via Protein kinase c theta (PKC- $\theta$ ) (and hence dormant) during activating but not inhibitory responses, within the first 5 min of NK cell activation. This phosphorylation is dynamic and increases along the progression of the inhibitory NKIS, while slightly decreasing during progression of the activating NKIS. SHP-1 phosphorylation dynamics were also closely correlated with changes in SHP-1 catalytic conformations. Blocking PKC- $\theta$ -mediated phosphorylation of SHP-1 restored SHP-1 activity and inhibited NK cell activation. Furthermore, NK cells bearing a phosphor-mimetic point mutation that suppresses SHP-1 activity at the serine 591 residue were highly activated. Finally, knockout of SHP-1 in NK cells rescued PKC- $\theta$  silencing and promoted tumor clearance in vivo. The PKC- $\theta$ -mediated

regulation of SHP-1 potentially serves to maintain and prime NK cells in a complex cellular environment consisting of both healthy and malignant cells, requiring finely tuned localized NK cell activity.

## Results

### SHP-1 S591 phosphorylation in NK cells is a dynamic process, differentially regulated during inhibitory and activating interactions

It remains unclear how SHP-1 activity is regulated throughout the duration of the NK cell response and how this regulation is maintained in different states, that is, during NK cell activation and inhibition. Furthermore, SHP-1 is recruited to both cytolytic and non-cytolytic NK synapses, demonstrating that different modes of regulation are needed to ensure proper NK cell responses (Vyas *et al.*, 2001; Vyas *et al.*, 2002a). Phosphorylation of SHP-1 was previously shown in different cellular systems (Li *et al.*, 1995; Jones *et al.*, 2004; Liu *et al.*, 2007). The outcome of these molecular processes, however, demonstrated contradictory results, and the molecular regulation of SHP-1 in NK cells has not been fully addressed. We recently employed a mutant YTS-2DL1 knock-in line expressing the SHP-1 phosphor-mimetic serine to aspartic acid residue substitution (SHP-1 S591D), which exhibits increased antitumor NK function relative to WT SHP-1-expressing YTS cells (Ben-Shmuel *et al.*, 2021). To dissect the possible effect of SHP-1 phosphorylation on NK cell function, physiological activating and inhibiting interactions were induced with 721.221 target cells, and S591 phosphorylation patterns were examined in YTS-2DL1 cells and isolated primary NK cells expressing KIR2DL1<sup>+</sup> (referred to as pNK-2DL1) from healthy human donors. We conducted functional assays as previously described (Matalon *et al.*, 2016; Matalon *et al.*, 2018) by incubating YTS-2DL1 or pNK-2DL1 with 721.221 target cells either expressing the KIR2DL1 cognate ligand, HLA Cw4 (721-Cw4, which inhibits NK activity), or an irrelevant HLA Cw7 ligand (721-Cw7 or 721-HLA-negative cells [Münz *et al.*, 1997], which promote NK cell activation). Cell lysates were immunoblotted (IB) with anti-pSHP-1 S591 antibody. Our data revealed different SHP-1 phosphorylation profiles during NK cell inhibition and activation after 5 min of incubation (Figure 1A). High S591 phosphorylation levels could be seen during activating interactions ( $3.06 \pm 0.31$ ,  $p=0.0104$ ), whereas lower SHP-1 S591 phosphorylation was observed during induced inhibitory interactions. The same pattern was observed during incubation of pNK-2DL1 cells with activating 721-HLA-negative cells or with inhibiting 721-Cw4 targets cells ( $2.51 \pm 0.19$ ,  $p=0.006$ , Figure 1B). The formation of the immunological synapse (IS) is highly dynamic, involving movement, activation, and termination of signaling complexes (Burroughs and Wülfing, 2002). Therefore, we wished to analyze the change in SHP-1 S591 phosphorylation over time. YTS-2DL1 or pNK-2DL1 cells were incubated with activating or inhibiting 721.221 targets for 5, 10, 15, and 20 min. Strikingly, we found that pS591 on SHP-1 was dramatically altered during formation of the inhibitory NKIS, showing almost no initial phosphorylation after 5 min of incubation, and displaying high phosphorylation by 20 min. Activating NK cell interactions, however, displayed higher SHP-1 S591 phosphorylation during the first 5 min of activation, remaining relatively stable, with a slight (nonsignificant) reduction after 20 min of activation (Figure 1C, Figure 1—figure supplement 1). Collectively, these results suggest that SHP-1 S591 phosphorylation may play a role during NK cell activation and during late inhibitory interactions. This mechanism may attenuate SHP-1 functionality in order to enable NK cell activation within these time frames.

### SHP-1 conformational kinetics parallel S591 phosphorylation patterns

To elucidate whether SHP-1 phosphorylation on the S591 residue complements SHP-1 conformation and activation status, an SHP-1 Förster resonance energy transfer (FRET) biosensor construct was cloned into YTS-2DL1 cells as we previously described (Matalon *et al.*, 2018). The FRET sensor was constructed with SHP-1 tagged on the N' and C' termini with YFP and CFP, respectively (YFP-SHP-1-CFP). It is known that SHP-1 activation status is correlated with its conformation (Poole and Jones, 2005; Wang *et al.*, 2011). In the closed conformation, the N' SH2 domain masks the catalytic domain rendering the enzyme inactive, whereas when the catalytic domain is free of the N' SH2 domain, the protein remains in an open active conformation (Wang *et al.*, 2011). Hence, an inactive SHP-1 protein provides high FRET efficiency due to YFP and CFP proximity, and an active SHP-1 protein demonstrates low FRET efficiency as SHP-1 is in an open conformation, distancing the two reporter proteins. With this construct, we could image the dynamic activation and inhibition status of SHP-1 throughout

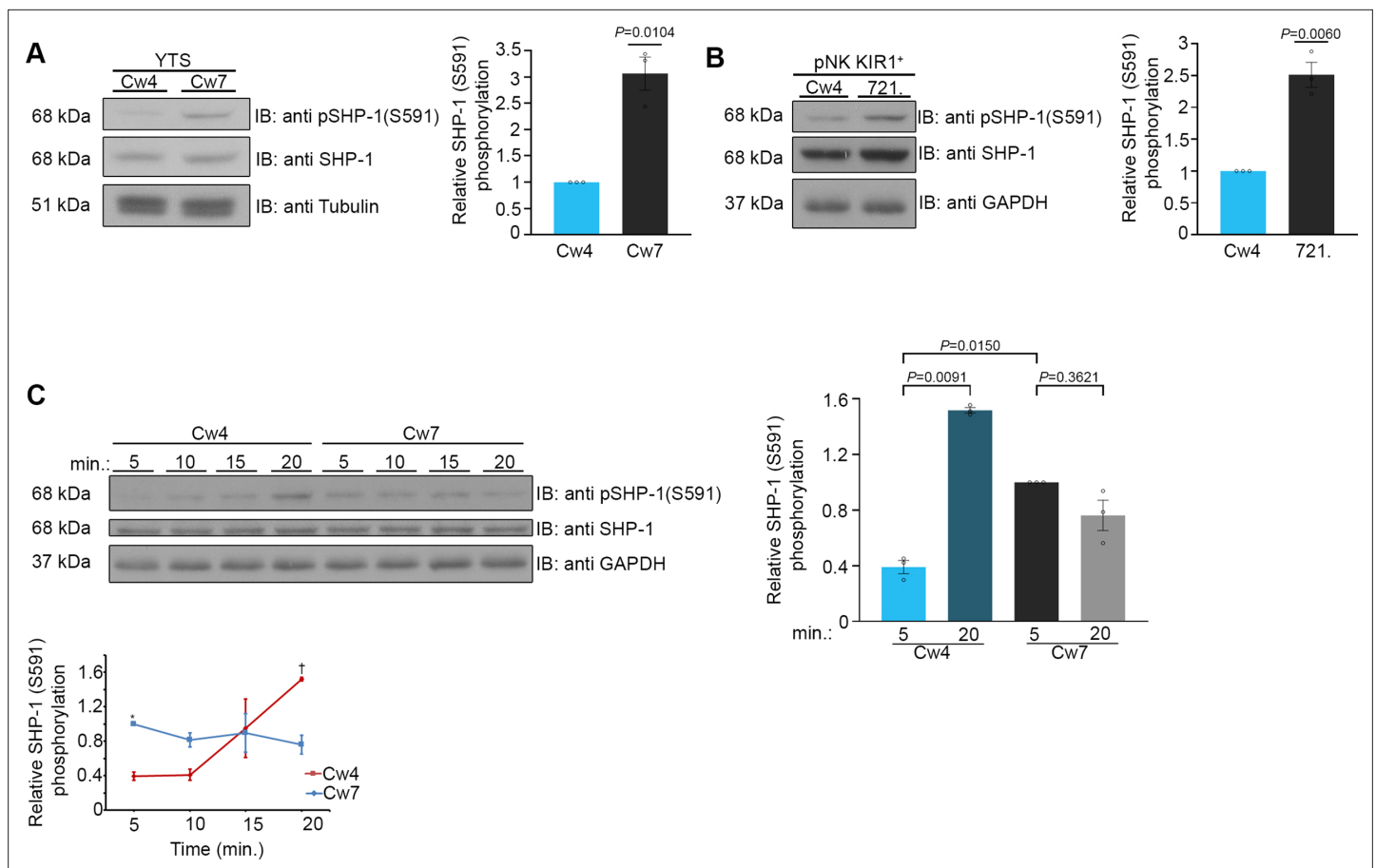


**Figure 1.** Phosphorylation kinetics of SHP-1 S591 during activating and inhibitory NK cell interactions. **(A)** YTS-2DL1 NK cells were incubated with either inhibitory 721-Cw4 HLA or activating 721-Cw7 HLA target cells at 37°C for 5 min, and then lysed. Lysates were separated on SDS-PAGE and immunoblotted with anti-pSHP-1 S591 antibody. SHP-1 S591 phosphorylation levels were measured by densitometric analysis, relative to  $\beta$ -tubulin loading control using ImageJ. Samples were normalized to the YTS-2DL1 sample incubated with 721-Cw4 target after 5 min of activation ( $p=0.0104$ , quantification on the right showing the average of three independent experiments). **(B)** pNK-2DL1 cells were incubated with either 721-Cw4 HLA or 721-HLA-negative target cells at 37°C for 5 min. pSHP-1 S591 levels were determined as in **(A)** ( $p=0.0060$ , quantification on the right showing the average of three independent experiments). **(C)** YTS-2DL1 cells were incubated with target cells as described in **(A)**, for four different time points, as indicated. pSHP-1 S591 levels were quantitated as in **(A)**. Statistical significance between Cw4 and Cw7 after 5 min of activation ( $p=0.015$ ), statistical significance between Cw4 at 5 min versus 20 min ( $p=0.0091$ ). pSHP-1 S591 levels of YTS-2DL1 cells incubated with targets for 5 and 20 min are shown in the bar graph (quantification showing the average of three independent experiments). Data are shown as mean  $\pm$  SEM. One-sample t-tests **(A, B)** or one-way ANOVA with Tukey test **(C)** was used to calculate p-values.

The online version of this article includes the following source data and figure supplement(s) for figure 1:

**Source data 1.** Representative blots.

**Source data 2.** Numerical data for all the graphical presentations in **Figure 1**.

**Figure supplement 1—source data 1.** Numerical data for the graphical presentation in **Figure 1—figure supplement 1**.

**Figure supplement 1.** Phosphorylation kinetics of SHP-1 S591 in pNK cells.

the lifetime of the NKIS as previously reported (*Matalon et al., 2018*). YTS-2DL1 cells were transfected with the YFP-SHP-1-CFP FRET sensor construct and incubated with inhibiting 721-Cw4 or activating 721-Cw7 cells stably expressing mCherry in order to distinguish NK and target cells. FRET efficiency was measured using high-resolution microscopy, as previously described (*Barda-Saad et al., 2005; Pauker et al., 2012; Fried et al., 2014*). In this set of experiments, we chose to focus on very early (5 min) and late (20 min) stages of NK cell: target cell interactions, as they showed the largest change in SHP-1 S591 phosphorylation (**Figure 1, Figure 1—figure supplement 1**). FRET measurements demonstrated patterns similar to SHP-1 S591 phosphorylation profiles; during initial inhibitory NK:721-Cw4 interactions (5 min), SHP-1 in NK cells displayed low synaptic FRET efficiency, indicating

an open and active state ( $8.62\% \pm 1.8\%$ ), shifting to high FRET efficiency after 20 min of synapse maturation ( $15.13\% \pm 1.9\%$ ,  $p=0.0300$ ; **Figure 2A and B**, top two panels), indicating a closed and inhibited state. During activating interactions, however, SHP-1 in NK cells displayed highest synaptic FRET efficiency after 5 min ( $18.45\% \pm 1.9\%$ ,  $p=0.0003$  comparing 5 min of activation to inhibition), indicating a closed and inhibited state, while after 20 min of activation, a decrease was observed in SHP-1 FRET efficiency to similar levels as NK:721-Cw4 interactions after 5 min ( $8.15\% \pm 1.9\%$ ,  $p=0.006$ ; **Figure 2A and B**, bottom two panels), indicating an open and active SHP-1 conformation (**Matalon et al., 2018**). These data demonstrate that SHP-1 conformation, and accordingly, its activation status, changes differentially during activating and inhibiting interactions as the NKIS matures, correlating with S591 phosphorylation patterns. Our results suggest that SHP-1 conformation and catalytic activation are regulated in a temporal manner at both the activating and inhibitory NKIS, and suggest a possible role for SHP-1 S591 phosphorylation on SHP-1 activity in NK cells.

### pSHP-1 distinguishes between NK cell-activating and -inhibiting synapses, and correlates with PKC- $\theta$ accumulation at the NKIS

In transformed tissues, NK cells interact with both susceptible targets and bystander cells, which may both influence NK cell function (**Zhou et al., 2017**). NK cells are capable of serial cytotoxicity and rapidly engage with and detach from these different targets (**Choi and Mitchison, 2013; Forslund et al., 2015; Guldevall et al., 2016**). It was recently demonstrated that NKIS maintenance is highly regulated, and signaling events that lead to NK cell attachment to new target cells accelerate the detachment from previous targets (**Netter et al., 2017; Srpan et al., 2018**). Furthermore, highly regulated lytic granule convergence to the microtubule organizing center (MTOC) is crucial for NK cells to avoid bystander cell killing (**Hsu et al., 2016**). Thus, it is evident that controlled and coordinated signaling events are critical for NK cell target identification and subsequent precise function.

We hypothesized that SHP-1 S591 phosphorylation may thus enable rapid discrimination by NK cells between healthy and malignant targets, facilitating controlled and sequential killing in a heterogeneous environment. To examine whether SHP-1 phosphorylation in NK cells is coordinately directed when NK cells are challenged simultaneously with activating and inhibitory signals, pNK-2DL1 cells were concurrently incubated with both activating K562-CFP and inhibiting 721-Cw4-mCherry stably labeled cells. Synapse intensity of pSHP-1 S591 was assessed in NK cells that were found forming simultaneous dual synapses with both activating and inhibiting cells. Strikingly, NK cells were able to rapidly distinguish between activating and inhibitory targets cells as measured by higher pSHP-1 S591 levels that were localized to synapses with K562, versus 721-Cw4 cells (**Figure 3A**,  $p=0.0074$ ). Hence, SHP-1 S591 phosphorylation is a regulated and directed event and may allow NK cells to locally regulate SHP-1 phosphorylation to enable the maintenance of multiple local activation states in a single cell.

We next aimed to identify the serine kinase implicated in SHP-1 S591 phosphorylation. PKC- $\theta$  is expressed predominantly in hematopoietic and muscle cells (**Osada et al., 1992; Baier et al., 1993**), and was shown to play multiple roles in T cell activation (**Hayashi and Altman, 2007**). In human NK cells, the role and molecular pathways of PKC- $\theta$  are incompletely defined. PKC- $\theta$  was suggested to participate in murine NK cell activity (**Tassi et al., 2008; Aguiló et al., 2009; Anel et al., 2012; Merino et al., 2012**); however, the mechanism by which it exerts this function remains unclear. It was shown that TNF- $\alpha$  and IFN- $\gamma$  secretion is defective in PKC- $\theta^{-/-}$  mice (**Page et al., 2008**), and this can contribute to defective recruitment of effector cells to the site of tumor development. In a different study (**Tassi et al., 2008**), no effect of PKC- $\theta$  deficiency was observed on IFN- $\gamma$  secretion induced by IL-12, IL-18, or a combination of both cytokines. Therefore, it is not clear how PKC- $\theta$  is involved in the regulation of NK cell signaling cascades, and if its activity impacts human NK cell function.

Early reports by Vyas et al. showed that PKC- $\theta$  localizes to the cytolytic NK synapse during early activation, that is, following 5 and 10 min of activating target cell conjugation, and relatively low PKC- $\theta$  polarization is observed following 10 min of non-cytolytic NK: target cell conjugates (**Vyas et al., 2002a**). This PKC- $\theta$  localization was similar to the localization of SHP-1 at the NKIS. Thus, we next studied PKC- $\theta$  dynamics in NK cell inhibitory synapses and how these compare to PKC- $\theta$  localization during NK cell activation. Moreover, since PKC- $\theta$  plays a role in activation of different hematopoietic cells (**Baier et al., 1993; Hayashi and Altman, 2007**) and induces SHP-1 S591 phosphorylation during T cell activation (**Liu et al., 2007**), we tested its possible interplay with SHP-1 in NK cells. YTS-2DL1

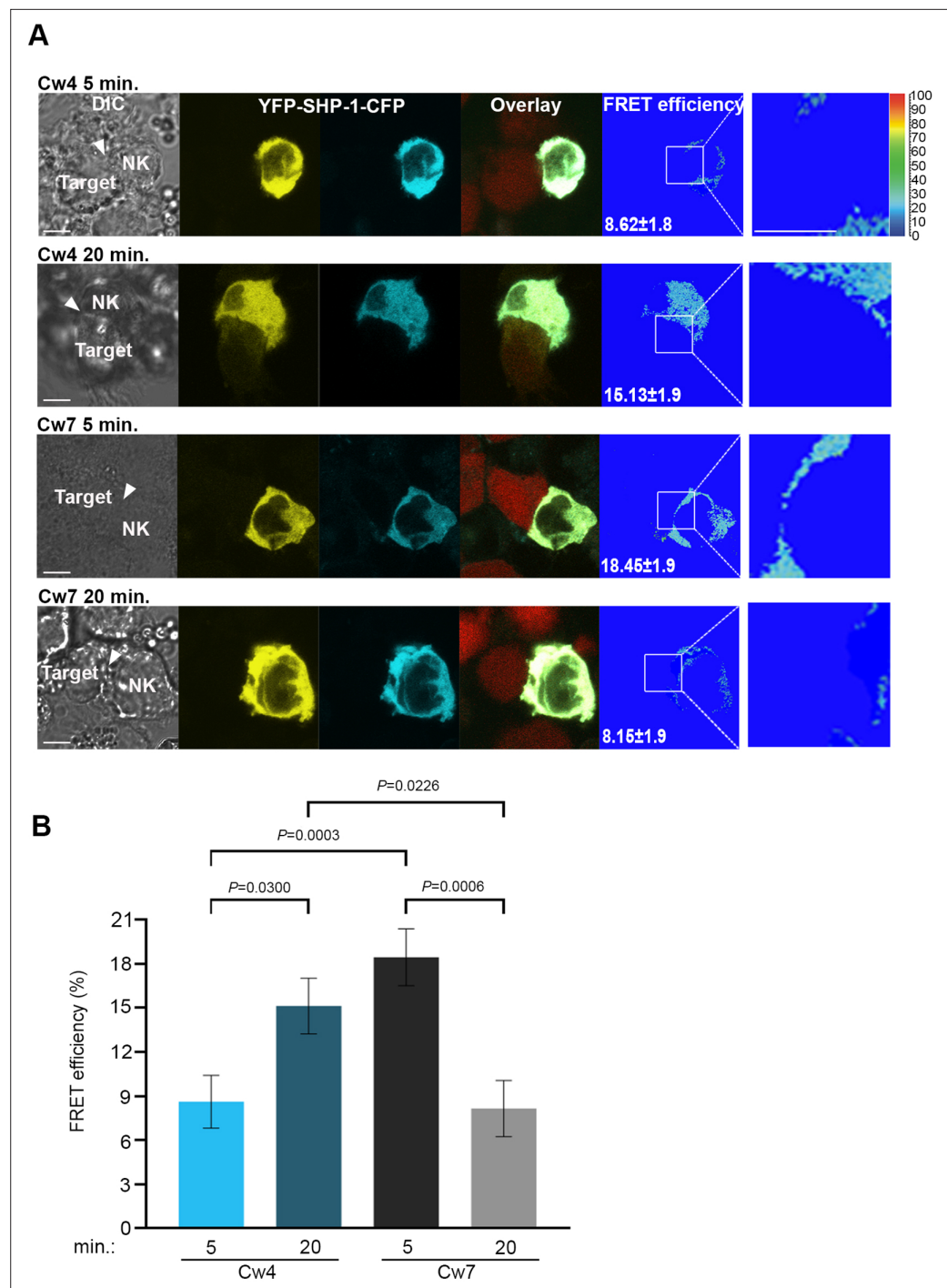


**Figure 2.** SHP-1 conformational dynamics reflect S591 phosphorylation during activating and inhibitory NK cell interactions. **(A)** YTS-2DL1 YFP-SHP-1-CFP cells were incubated over slides pre-seeded with 721-Cw4 (top panels) or Cw7 (bottom panels) target cells expressing mCherry. The cells were incubated for 5 or 20 min at 37°C to enable conjugate formation, and fixed. FRET analysis was performed as indicated. **(B)** Graph summarizing FRET efficiency following 5 or 20 min activation with Cw4 or Cw7 target cells. For Cw4, 5 and 20 min activation,  $n = 72$  and  $62$  cell conjugates analyzed, respectively. For Cw7, 5 and 20 min activation,  $n = 73$  and  $47$  cell conjugates analyzed from three independent experiments, respectively. Data are shown as mean  $\pm$  SEM. Two-way ANOVA with Tukey test **(B)** was used to calculate p-values.

The online version of this article includes the following source data for figure 2:

**Source data 1.** Numerical data for all the graphical presentations in **Figure 2**.

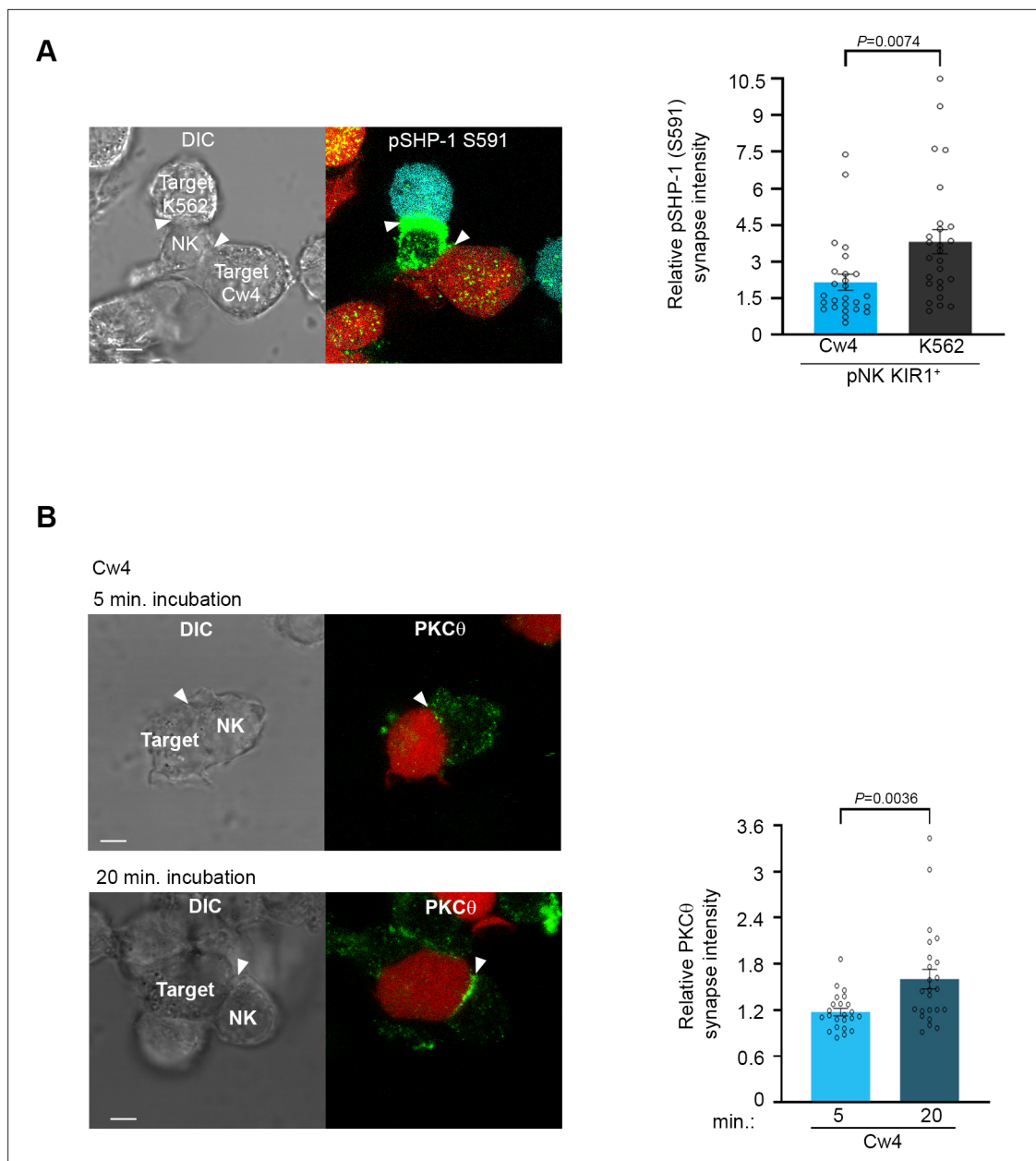


**Figure 3.** Phosphorylation of SHP-1 S591 occurs at the activating NKIS during simultaneous activating and inhibitory synapse formation, in parallel to PKC- $\theta$  accumulation. **(A)** pNK-2DL1 cells were incubated over slides pre-seeded with 721-Cw4 and K562 cells expressing mCherry or CFP, respectively. The cells were incubated for 5 min at 37°C to enable conjugate formation and were fixed. pSHP-1 S591 was labeled with primary rabbit anti-pSHP-1 S591 antibody, and secondary anti-rabbit 488 antibody. Synapse intensity was quantified in NK cells relative to each cell in multiple NK cell synapses with two different targets ( $p=0.007$ , quantification on the right of triple-cell conjugates collected,  $n=26$ ). **(B)** YTS-2DL1 cells were incubated over slides pre-seeded with 721-Cw4 target cells expressing mCherry. The cells were incubated for 5 or 20 min at 37°C to enable conjugate formation and were fixed. PKC- $\theta$  was subsequently labeled with primary goat anti-PKC- $\theta$  antibody and secondary anti-goat 488 antibody. Right: graph summarizing PKC- $\theta$  accumulation at the NKIS at two time points following activation. Analysis was conducted comparing PKC- $\theta$  intensity at the NKIS relative to the rest of the NK cell. For Cw4, 5 and 20 min activation,  $n=24$  cell conjugates were analyzed from three independent experiments. Data are shown as mean  $\pm$  SEM. One-sample  $t$ -tests (**A**, **B**) were used to calculate  $p$ -values.

The online version of this article includes the following source data and figure supplement(s) for figure 3:

**Source data 1.** Numerical data for all graphical presentations in **Figure 3**.

**Figure supplement 1.** PKC- $\theta$  accumulation at the activating NKIS.

**Figure supplement 1—source data 1.** Numerical data for the graphical presentation in **Figure 3—figure supplement 1**.

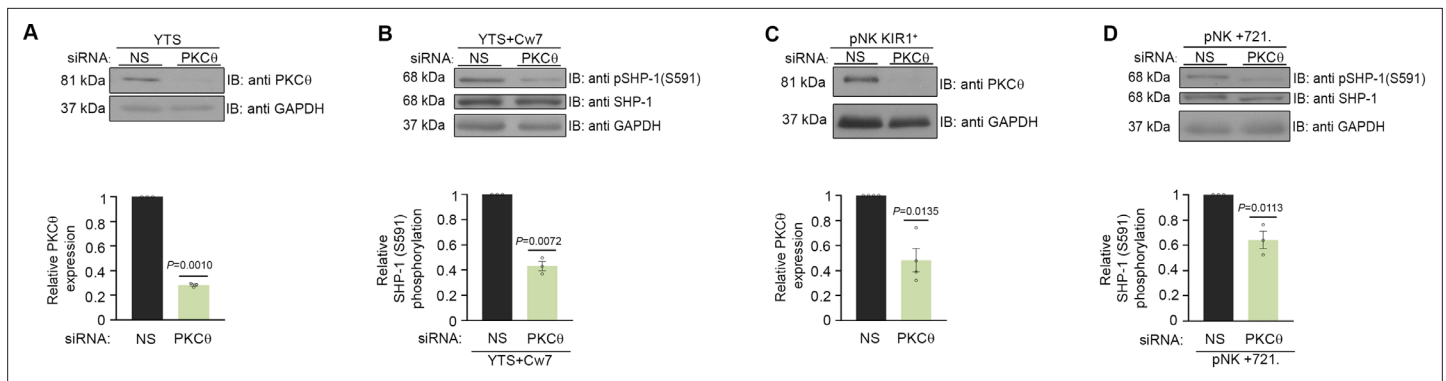


**Figure 4.** SHP-1 phosphorylation is mediated through PKC- $\theta$ . **(A)** Silencing efficiency of PKC- $\theta$ . YTS-2DL1 cells treated with either nonspecific (control) (NS) or PKC- $\theta$  siRNA, lysed, separated on SDS-PAGE, and immunoblotted with anti- PKC- $\theta$  antibody. PKC- $\theta$  levels were measured by densitometric analysis, relative to the GAPDH loading control using ImageJ. Samples were normalized to the sample treated with NS siRNA ( $p=0.001$ , quantification on the bottom showing average of three independent experiments). **(B)** YTS-2DL1 treated with either NS or PKC- $\theta$  siRNA were incubated with 721-HLA target cells at 37°C for 5 min, and cells were subsequently lysed. Lysates were separated on SDS-PAGE, transferred to a nitrocellulose membrane, and immunoblotted with anti-pSHP-1 S591 antibody. SHP-1 S591 phosphorylation levels were measured by densitometric analysis, relative to the GAPDH loading control using ImageJ. Samples were normalized to the YTS-2DL1 sample treated with NS siRNA and incubated with 721-Cw7 targets ( $p=0.0072$ , quantification on the bottom of independent experiments,  $n = 3$ ). **(C)** Silencing efficiency of PKC- $\theta$ . pNK-2DL1 cells were transfected with 250 pmol of PKC- $\theta$  siRNA. After 48 hr, prior to incubation with target cells, pNK-2DL1 were counted and lysed. Lysates were separated on SDS-PAGE and immunoblotted with anti-PKC- $\theta$  antibody. PKC- $\theta$  expression levels were measured by densitometric analysis using ImageJ and expressed relative to the GAPDH loading control. Samples were normalized according to the pNK-NS siRNA sample. Bar graph on the bottom shows the average of three independent experiments. **(D)** pNK-2DL1 cells were incubated with 721-HLA-negative cells at 37°C for 5 min, and cells were subsequently lysed. Lysates were separated on SDS-PAGE and transferred to a nitrocellulose membrane that was immunoblotted with anti-pSHP-1 S591 antibody. SHP-1 S591 phosphorylation levels were measured by densitometric analysis, relative to the GAPDH loading control using ImageJ. Samples were normalized to the pNK-2DL1 sample treated with NS siRNA and incubated with 721 targets ( $p=0.0113$ , quantification on the bottom showing the average of three independent experiments). Data are shown as mean  $\pm$  SEM. One-sample t-tests (**A–D**) were used to calculate p-values.

The online version of this article includes the following source data for figure 4:

**Source data 1.** Representative blots.

**Source data 2.** Numerical data for all the graphical presentations in **Figure 4**.

NK cells were incubated with mCherry-labeled 721-Cw4 target cells for either 5 (early) or 20 (late) min (**Figure 3B**). PKC- $\theta$  localization appeared dispersed at the early inhibitory NKIS and accumulated at the synapse after 20 min ( $p=0.0036$ ). These dynamics were similar to SHP-1 S591 phosphorylation patterns. Furthermore, we observed PKC- $\theta$  accumulation at the activating NKIS at the initial time point, which did not significantly decrease after 20 min (**Figure 3—figure supplement 1**,  $p=0.5068$ ). This suggested that PKC- $\theta$  may play a role in regulating late inhibitory and early activating signaling pathways via SHP-1 regulation.

These data suggest that PKC- $\theta$  plays a role in human NK cell activation, and possibly in late (20 min) NK cell inhibition, potentially through SHP-1 regulation at the late inhibitory NKIS, and throughout the lifetime of the activating NKIS (5–20 min).

### SHP-1 phosphorylation on S591 is facilitated through PKC- $\theta$

In order to determine whether SHP-1 S591 phosphorylation is mediated through PKC- $\theta$  in NK cells, a specific small interfering RNA (siRNA) gene silencing approach was utilized in YTS-2DL1 and pNK-2DL1 cells. Cells were gene-silenced for PKC- $\theta$  and incubated with 721.221 target cells (**Figure 4**). Significant silencing efficiency was obtained in all experiments ( $p=0.001$  and  $p=0.0135$  for YTS and pNK-2DL1 cells, respectively) relative to cells transfected with nonspecific (NS) siRNA control (**Figure 4A and C**).

Next, SHP-1 S591 phosphorylation levels were examined in YTS-2DL1 and pNK-2DL1 cells that were treated with NS siRNA vs. PKC- $\theta$  siRNA and incubated with 721-Cw7 or 721-HLA-negative target cells in order to elucidate the role of PKC- $\theta$  on SHP-1 S591 phosphorylation during stimulation. Though S591 phosphorylation was not completely eliminated, a reduction in SHP-1 S591 phosphorylation levels could be seen in YTS-2DL1 or pNK-2DL1 treated with PKC- $\theta$  siRNA as opposed to NS



siRNA (by 2.5-fold  $\pm$  0.03,  $p=0.0072$ ; by 1.7-fold  $\pm$  0.07,  $p=0.0113$ , respectively) (**Figure 4B and D**). Together, these data demonstrate PKC- $\theta$  involvement in SHP-1 S591 phosphorylation in NK cells.

## PKC- $\theta$ regulates SHP-1 conformation status and its enzymatic activity at the NKIS

To determine whether SHP-1 conformation is affected by PKC- $\theta$ , YTS-2DL1 cells were co-transfected with YFP-SHP-1-CFP along with NS or PKC- $\theta$ -specific siRNA and incubated with targets for 5 min. Synaptic FRET efficiency was significantly reduced in YTS-2DL1 YFP-SHP-1-CFP cells pretreated with PKC- $\theta$  siRNA versus NS siRNA (18.5%  $\pm$  2.04% vs. 9.8%  $\pm$  1.7%,  $p=0.0025$ ), suggesting that the SHP-1 in the silenced cells acquires the open conformation (**Figure 5A and B**). Interestingly, PKC- $\theta$  gene silencing reduced the FRET efficiency of YFP-SHP-1-CFP in the activating NKIS to similar FRET levels observed in YTS-2DL1 YFP-SHP-1-CFP cells pretreated with NS siRNA following inhibitory interactions (5.76%  $\pm$  1.6% vs. 9.8%  $\pm$  1.7%,  $p=0.2663$ ) (**Figure 5A and B**). Hence, although the SHP-1 conformation in activating synapses is closed and inactive, PKC- $\theta$  gene silencing increases SHP-1 open and active conformation at the activating NKIS, as detected by reduced FRET efficiency between the N' and C' termini of the SHP-1 sensor. This may suggest a role for PKC- $\theta$  in reducing SHP-1 activity at the activating NKIS, where SHP-1 localizes yet is inactive, and possibly during the termination of the inhibitory synapse to enable subsequent NK cell activity.

In order to examine whether the altered SHP-1 conformation induced under PKC- $\theta$  gene silencing affects SHP-1 catalytic activity, SHP-1 activity was assessed through PTP assay. Direct catalytic activity of SHP-1 on the pNPP substrate was shown to be higher in cells treated with PKC- $\theta$  siRNA rather than in cells treated with NS siRNA (81%  $\pm$  3.3% vs. 65%  $\pm$  3% activity,  $p=0.0246$ ) (**Figure 5—figure supplement 1**). Collectively, these results indicate that SHP-1 phosphorylation by PKC- $\theta$  can shift the SHP-1 conformational state from open (active) to closed (inactive), and thus reduce SHP-1 enzymatic activity.

## SHP-1 activity is modified under PKC- $\theta$ -mediated regulation

To further characterize the ability of PKC- $\theta$  to regulate SHP-1 catalytic activity, the phosphorylation profile of key signaling proteins that serve as SHP-1 substrates was compared following NK cell activation or inhibition under PKC- $\theta$  gene silencing. SHP-1 was shown to dephosphorylate VAV1 as a mechanism of terminating NK cell activation (**Stebbins et al., 2003**). Furthermore, our recent studies identified novel SHP-1 substrates including PLC $\gamma$ 1/2 and LAT (**Matalon et al., 2016**).

We therefore examined how PKC- $\theta$  gene silencing affects SHP-1 catalytic activity on its substrates in YTS and pNK-2DL1 cells. In order to assess the phosphorylation status of these proteins, cells were treated with either PKC- $\theta$  siRNA or NS siRNA and incubated with inhibitory Cw4-721 or activating Cw7-721 or 721-HLA-negative target cells. IB (immunoblotted) of pVAV1 (Y160) revealed an approximately twofold reduction in phosphorylation levels in activated YTS-2DL1 samples treated with PKC- $\theta$  siRNA in contrast to NS siRNA ( $p=0.0001$ ) (**Figure 6A**). Similarly, pNK-2DL1 cells demonstrated a similar reduction in pVAV1 (Y160) phosphorylation levels subsequent to PKC- $\theta$  gene silencing ( $p=0.0192$ ) (**Figure 6A**). Furthermore, phosphorylation of VAV1 in activating interactions following PKC- $\theta$  gene silencing was similar to its phosphorylation during inhibitory interactions (YTS and pNK-2DL1 cells treated with NS siRNA). In addition to VAV1, pNK-2DL1 cells showed a 1.8-fold  $\pm$  0.2 reduction in pPLC $\gamma$ 1 levels ( $p=0.0032$ ) when treated with PKC- $\theta$  siRNA (**Figure 6B**). A similar trend can be seen in YTS-2DL1 cells in which immunoprecipitation (IP) of PLC $\gamma$ 1 and IB of pPLC $\gamma$ 1 (Y783) revealed a reduction of 1.4-fold  $\pm$  0.04 in pPLC $\gamma$ 1 levels following PKC- $\theta$  gene silencing under activating interactions ( $p=0.0074$ ) (**Figure 6E**). Together, these data suggest that PKC- $\theta$ -mediated regulation of SHP-1 catalytic activity may promote SHP-1 inactivation, and thus enhance NK cell reactivity.

In order to demonstrate that PKC- $\theta$  regulation of SHP-1 via S591 influences SHP-1 substrate phosphorylation and activation, and not PKC- $\theta$  silencing per se, a mutant YTS-2DL1 line expressing an SHP-1 mutant that mimics the constitutively phosphorylated state, SHP-1 S591D (referred to as YTS-2DL1 SHP-1 S591D), was created utilizing CRISPR/Cas9, as previously reported (**Ben-Shmuel et al., 2021**). In cells expressing this mutant, PKC- $\theta$  silencing would not be expected to impact SHP-1 activity (**Egelhoff et al., 1993; Huang and Erikson, 1994; Léger et al., 1997**). Hence, we expected that the S591D mutant would demonstrate high accumulation of pVAV1 in the synapse, irrespective of PKC- $\theta$  silencing. WT YTS-2DL1 or YTS-2DL1 SHP-1 S591D NK cells were treated with either NS or PKC- $\theta$

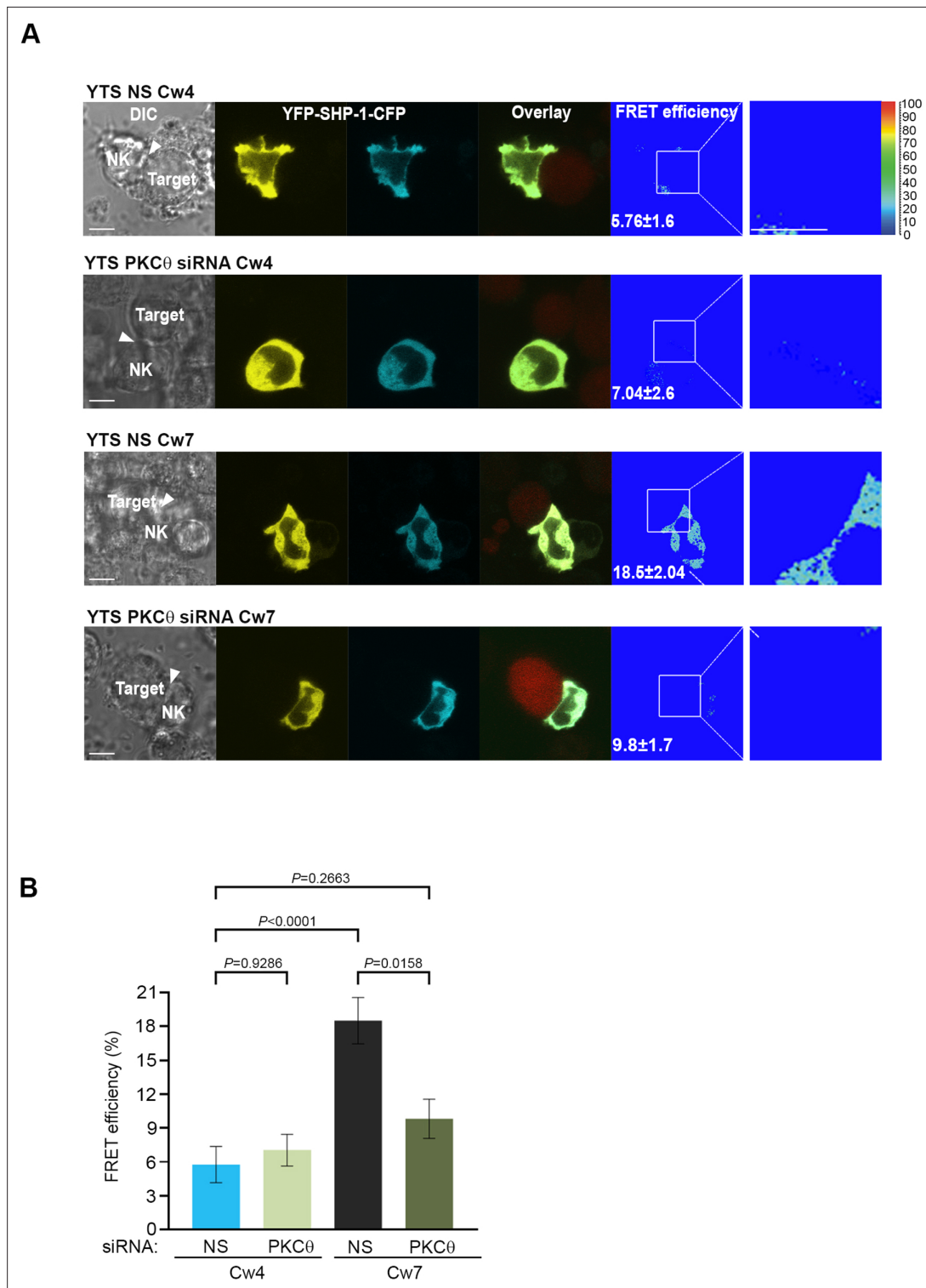


**Figure 5.** SHP-1 conformation is regulated by PKC- $\theta$  at the NKIS. **(A)** YTS-2DL1 YFP-SHP-1-CFP cells were treated with either NS or PKC- $\theta$  siRNA and incubated over slides pre-seeded with 721-Cw4 (top panels) or Cw7 (bottom panels) target cells expressing mCherry. The cells were incubated for 5 min at 37°C to enable conjugate formation and were fixed. FRET analysis was performed, as indicated. **(B)** Graph summarizing FRET efficiency during 5 min activation with 721-Cw4 or Cw7 target cells. For Cw4 NS and PKC- $\theta$  siRNA,  $n = 52$  and  $63$  cell conjugates were analyzed, respectively, and for Cw7 NS and PKC- $\theta$  siRNA  $n = 67$  and  $61$  cell conjugates were analyzed from three independent experiments, respectively. Data are shown as mean  $\pm$  SEM. Two-way ANOVA with Tukey test **(B)** was used to calculate p-values.

The online version of this article includes the following source data and figure supplement(s) for figure 5:

Figure 5 continued on next page

Figure 5 continued

**Source data 1.** Numerical data for all the graphical presentations in **Figure 5**.

**Figure supplement 1.** PKC- $\theta$  regulates SHP-1 activity.

**Figure supplement 1—source data 1.** Representative blot.

**Figure supplement 1—source data 2.** Numerical data for the graphical presentation in **Figure 5—figure supplement 1**.

siRNA, and incubated with mCherry-expressing target cells to assess pVAV1 Y160 synaptic accumulation. As expected, pVAV1 Y160 accumulation was observed during activating but not inhibitory NK cell interactions ( $p < 0.0001$ ), and in accordance with our results, PKC- $\theta$  siRNA-treated NK cells had a  $2 \pm 0.2$ -fold reduction in pVAV1 recruitment to the activating NKIS ( $p < 0.0001$ ), indicating increased SHP-1 activity in the absence of PKC- $\theta$  under activating interactions (**Figure 6C**). No significant decrease in pVAV1 recruitment was observed, however, in YTS-2DL1 SHP-1 S591D cells treated with either NS or PKC- $\theta$  siRNA under either activating or inhibitory interactions ( $p = 0.9109$  and  $p = 0.9999$ , respectively). Furthermore, YTS-2DL1 SHP-1 KO cells were reconstituted with either YFP-SHP-1 WT or with YFP-SHP-1 mutant constructs, including the constitutively phosphorylated SHP-1 mimetic (YFP-SHP-1 S591D, constitutively inactive) or an SHP-1 phospho-abolishing mutant (YFP-SHP-1 S591A, constitutively active). YTS-2DL1 SHP-1 KO cells transfected with the YFP-SHP-1 constructs were incubated with Cw4-721 targets expressing mCherry and stained for pPLC $\gamma$ 1 (Y783) (**Figure 6D**). We previously showed that pPLC $\gamma$ 1 (Y783) accumulation at the NKIS is favored during activating rather than inhibitory NK cell interactions (**Matalon et al., 2016**). Interestingly, cells expressing SHP-1 S591D showed high levels of pPLC $\gamma$ 1 (Y783) accumulation at the NKIS, even though the NKIS was inhibitory. These levels were approximately three-fold higher compared to YTS-2DL1 cells expressing SHP-1 WT or SHP-1 S591A ( $p < 0.0001$ ). Collectively, these results demonstrate that PKC- $\theta$  negatively regulates SHP-1 activity by phosphorylating S591, as demonstrated through higher VAV1 and PLC $\gamma$ 1 tyrosine phosphorylation, and accumulation at the NK synapse.

### PKC- $\theta$ -mediated regulation of SHP-1 augments NK cell activation

SHP-1 tunes NK cell activation, and, as we demonstrated here, PKC- $\theta$ -mediated phosphorylation of SHP-1 impacts its enzymatic activity. We therefore next determined the effect of PKC- $\theta$  regulation on NK cell effector function and activation. PKC- $\theta$  silencing in NK cells resulted in a decrease in the phosphorylation profile of VAV1 and PLC $\gamma$ 1 in a SHP-1-dependent manner (**Figure 6**). These data suggest that the PKC- $\theta$ :SHP-1 axis may affect NK cell activation and cytotoxicity in a manner that is highly dependent on calcium flux and actin reorganization (**Orange et al., 2002; Stebbins et al., 2003; Bryceson et al., 2006; Caraux et al., 2006; Upshaw et al., 2006; Andzelm et al., 2007; Kim et al., 2010; Dong et al., 2012; Mizesko et al., 2013; Carisey et al., 2018**). To this end, PKC- $\theta$  was gene-silenced in YTS-2DL1 cells, and intracellular calcium flux was measured in NK cells incubated with activating 721-Cw7 target cells. As expected, calcium flux levels were higher in activated vs. inhibited NK cells treated with NS siRNA (black vs. blue curve, **Figure 7A**). However, PKC- $\theta$  siRNA reversed this trend, reducing calcium flux levels during NK cell activation near the levels obtained during NK cell inhibition (green vs. blue curve, **Figure 7A**). Similar results were obtained in pNK-2DL1 cells transfected with NS or PKC- $\theta$  siRNA and incubated with activating 721-HLA-negative or 721-Cw4-expressing cells (**Figure 7—figure supplement 1**). These results are consistent with the reduced phosphorylation levels of the calcium regulator, PLC $\gamma$ 1 (**Figure 6B, D and E**).

To assess how the PKC- $\theta$ :SHP-1 regulation controls NK cell cytotoxic potential, YTS-2DL1 cells were gene-silenced for PKC- $\theta$  and incubated with 721-Cw4 or Cw7 target cells, and target cell lysis was measured through Met release assay [ $^{35}\text{S}$ ], a direct measurement of NK cell killing of cancerous cells (**Figure 7B**). Target cell death was significantly reduced in YTS-2DL1 samples that were gene-silenced for PKC- $\theta$  under activating interactions ( $22\% \pm 3\%$  vs.  $42\% \pm 0.4\%$ ,  $p = 0.0037$ ). In fact, activating target cells (Cw7) incubated with PKC- $\theta$ -silenced NK cells demonstrated lysis levels similar to those of inhibitory targets (Cw4) incubated with YTS-2DL1 cells treated with NS siRNA ( $22\% \pm 3\%$  vs.  $13\% \pm 2.7\%$ ,  $p = 0.1015$ ). These data were verified in human pNK-2DL1 cells treated with NS or PKC- $\theta$  siRNA ( $5.5\% \pm 1.6\%$  vs.  $18\% \pm 1.06\%$ ,  $p = 0.0021$ , and  $5.5\% \pm 1.6\%$  vs.  $10\% \pm 1.32\%$ ,  $p = 0.2$ ) (**Figure 7C, Figure 7—figure supplement 1**). To verify that absence of PKC- $\theta$  influences NK cell effector functions through SHP-1 activity, and that the effects of PKC- $\theta$  silencing are abrogated in the

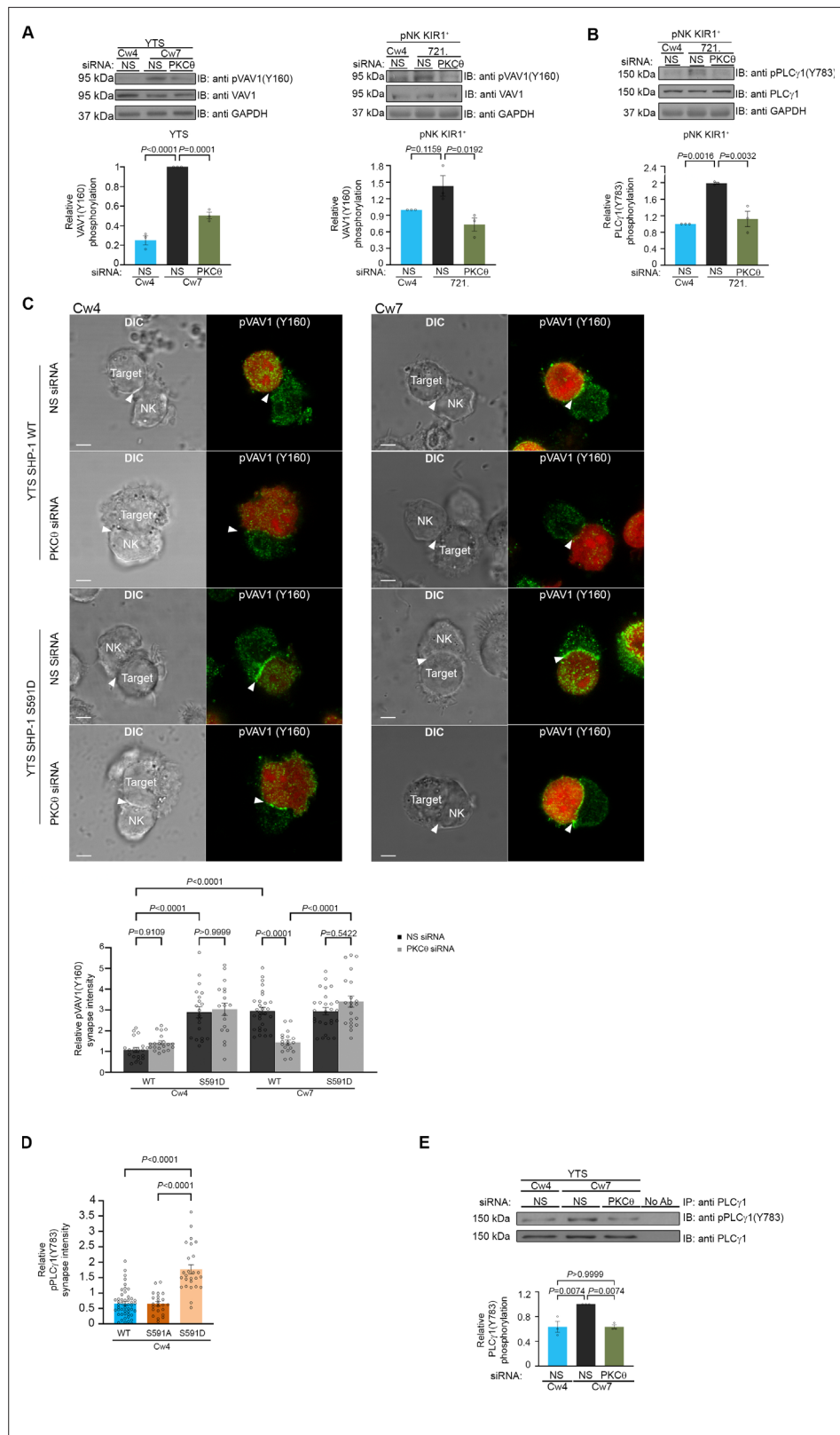


**Figure 6.** SHP-1 substrate phosphorylation is reduced following PKC- $\theta$  silencing. **(A)** YTS-2DL1 or pNK-2DL1 cells were transfected with 500 pmol of PKC- $\theta$  siRNA for 48 hr. Cells were incubated with target cells for 5 min at 37°C and then lysed. Lysates were separated on SDS-PAGE and immunoblotted with anti-pVAV-1 (Y160) antibody. Phosphorylation levels were measured by densitometric analysis, relative to the GAPDH loading control using

Figure 6 continued on next page

## Figure 6 continued

ImageJ. Samples were normalized according to the YTS-2DL1 or pNK-2DL1 NS siRNA Cw4 sample. Quantification of independent experiments is shown on the bottom;  $n = 3$  for YTS and  $n = 4$  for pNK experiments. **(B)** pNK-2DL1 cells were transfected with either NS or PKC- $\theta$  siRNA 48 hr prior to each experiment. Cells were incubated with either 721-Cw4 or 721-HLA-negative target cells for 5 min at 37°C, and subsequently lysed. Lysates were separated on SDS-PAGE and immunoblotted with anti-pPLC $\gamma$ -1 (Y783) antibody. Phosphorylation levels were measured by densitometric analysis, relative to the GAPDH loading control using ImageJ. Samples were normalized to the pNK-2DL1 NS siRNA Cw4 sample. Quantification of independent experiments is shown on the bottom;  $n = 3$ . The blot in **(A)** was stripped and reblotted against pPLC $\gamma$ 1(Y783) in **(B)**. **(C)** YTS-2DL1 WT or YTS-2DL1 SHP-1 S591D cells were transfected with either NS or PKC- $\theta$  siRNA and incubated over slides pre-seeded with 721-Cw4 or Cw7 target cells expressing mCherry. The cells were incubated for 5 min at 37°C to enable conjugate formation and fixed. pVAV-1 (Y160) was subsequently labeled with primary rabbit anti-pVAV-1 (Y160) antibody and secondary anti-rabbit 488 antibody. Quantification is shown on the bottom; for YTS-2DL1 WT NS or PKC- $\theta$  siRNA vs. Cw4 and Cw7,  $n = 21$  and 28 cell conjugates were analyzed, respectively. For YTS-2DL1 SHP-1 S591D NS or PKC- $\theta$  and Cw7,  $n = 21$  and 28 cell conjugates were analyzed from three independent experiments, respectively. **(D)** YTS-2DL1 SHP-1 KO cells were transfected with either WT YFP-SHP-1, YFP-SHP-1 S591A, or YFP-SHP-1 S591D phosphorylation mutants, and incubated on slides with mCherry-expressing 721-Cw4 target cells at 37°C. After 5 min incubation, the cells were fixed and stained with anti-pPLC $\gamma$ 1(Y783). NK cells were distinguished from targets based on mCherry expression by the target cells. Graph summarizes the relative synapse staining intensities. For WT YFP-SHP-1, YFP-SHP-1 S591A, and YFP-SHP-1 S591D,  $n = 48$ , 48, and 25 cell conjugates from three independent experiments analyzed, respectively. **(E)** YTS-2DL1 cells were transfected with either NS or PKC- $\theta$  siRNA 48 hr prior to the experiment. Cells were incubated with either 721-Cw4 or Cw7 target cells for 5 min at 37°C and subsequently lysed. Lysates were immunoprecipitated on beads containing PLC $\gamma$ -1 antibody and immunoblotted for pPLC $\gamma$ -1 (Y783). Densitometric analysis was normalized to PLC $\gamma$ -1 loading controls, and relative to the YTS-2DL1 NS siRNA: Cw7 pPLC $\gamma$ -1(Y783) sample. Bar graph on the bottom shows the average of three independent experiments. Data are shown as mean  $\pm$  SEM. One-way ANOVA with Tukey test **(A, B, D, E)** or two-way ANOVA with Tukey test **(C)** was used to calculate p-values.

The online version of this article includes the following source data for figure 6:

**Source data 1.** Representative blots.

**Source data 2.** Numerical data for all the graphical presentations in **Figure 6**.

absence of SHP-1, SHP-1 KO NK cells were additionally gene-silenced for PKC- $\theta$  (**Figure 7D**). Subsequently, WT and SHP-1 KO NK cells treated with either NS or PKC- $\theta$  siRNA were subjected to CD107a degranulation assay. As can be seen in **Figure 7D**, NK cells that were deficient in SHP-1 or both SHP-1 and PKC- $\theta$  displayed higher degranulation than WT cells ( $p=0.0127$  and  $p=0.0001$ ) and were not significantly affected by the presence or absence of PKC- $\theta$  ( $p=0.0603$ ). Furthermore, as shown in **Figure 7E**, PKC- $\theta$  knockdown also inhibits the NK cell-mediated antitumor response against 721-Cw7 cells as demonstrated by reduced NK cell degranulation compared to YTS-2DL1 cells treated with NS siRNA ( $p=0.0040$ ). Additionally, YTS-2DL1 SHP-1 S591D and YTS-2DL1 SHP-1 KO cells treated with NS or PKC- $\theta$  siRNA demonstrated restored degranulation ( $p=0.04$ ) against activating target cells, suggesting that antitumor responses were rescued by the absence of SHP-1 or the SHP-1 mutation at the PKC- $\theta$  phosphorylation site. Collectively, these data demonstrate that PKC- $\theta$  negatively regulates SHP-1 conformational state and activity, thereby providing a mechanism for maintaining NK cell activation and cytotoxic potential.

### SHP-1-deficient NK cells are unaffected by PKC- $\theta$ silencing and promote superior antitumor clearance relative to WT cells

We recently demonstrated that abrogation of SHP-1 activity in engineered NK cells can have enhanced benefits for NK-based immunotherapeutic approaches (**Ben-Shmuel et al., 2021**). Furthermore, it was recently shown that lower abundance of SHP-1 in NK cells enhances their tumoricidal capacity (**Wu et al., 2021**). To verify that NK cells silenced for PKC- $\theta$  have lower antitumor cytotoxicity due to enhanced SHP-1 activity, and not due to the absence of PKC- $\theta$  per se, non-obese diabetic (NOD) Rag1<sup>null</sup>IL2R $\gamma$ <sup>null</sup> (NRG) and NOD-SCID IL2R $\gamma$ <sup>null</sup> (NSG) mice were subcutaneously engrafted with 721-Cw4 or 721-Cw7 tumor cells, and injected with either  $5 \times 10^6$  WT YTS-2DL1, WT YTS-2DL1 gene-silenced for PKC- $\theta$ , YTS-2DL1 SHP-1KO cells (**Matalon et al., 2018**), YTS-2DL1 SHP-1KO cells that were gene-silenced for PKC- $\theta$  or YTS-2DL1 SHP-1 S591D mutant cells (**Ben-Shmuel et al., 2021**),

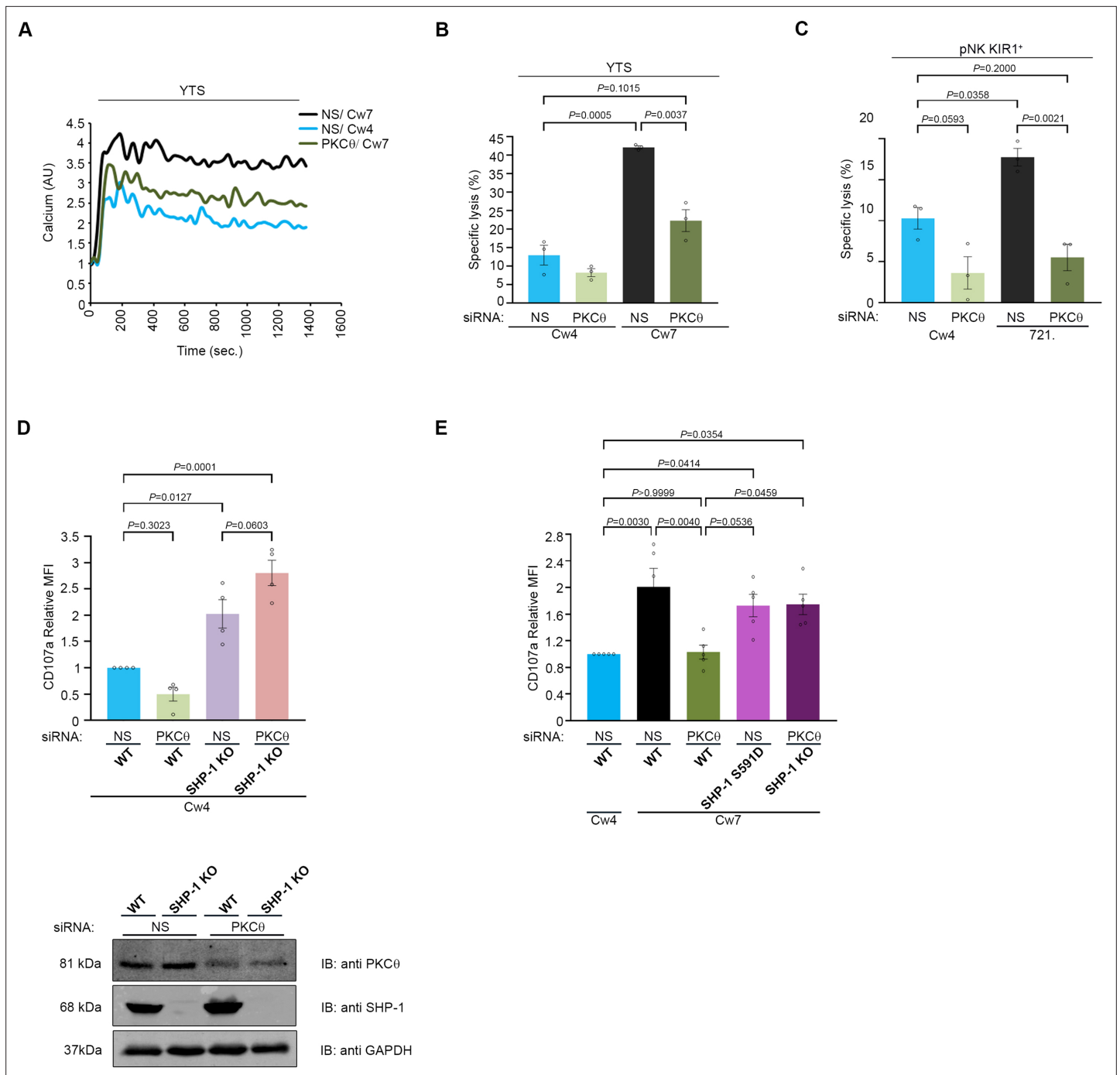


**Figure 7.** NK cell activation threshold is increased following gene silencing of PKC- $\theta$ . YTS-2DL1 cells were transfected with specific PKC- $\theta$  siRNA or with NS siRNA and assessed for effector activity after 48 hr. **(A)** YTS-2DL1 cells were loaded with calcium-sensitive Fluo-3-AM and analyzed for basal intracellular calcium levels for 1 min. The NK cells were then mixed with 721-Cw4 or Cw7 target cells and incubated at 37°C and analyzed by spectrofluorometry. **(B)** YTS-2DL1 cells were incubated with [<sup>35</sup>S]Met-labeled 721-Cw4 or Cw7 target cells at a ratio of 10:1 for 5 hr at 37°C. The specific lysis of target cells was measured. The graph summarizes three independent experiments. **(C)** pNK-2DL1 cells were incubated with [<sup>35</sup>S]Met-labeled 721-Cw4 or HLA-negative target cells at a ratio of 10:1 for 5 hr at 37°C. The specific target cell lysis was measured. The graph shows the average of three independent experiments. **(D)** WT YTS-2DL1 or YTS-2DL1 SHP-1 KO cells were treated with either NS or PKC- $\theta$ -specific siRNA 24 hr before incubation with mCherry-expressing 721-Cw4 target cells for 2 hr at 37°C, and analyzed for degranulation via FACS relative to the WT NS-treated cells incubated with 721-Cw4 targets, as described in Materials and methods. A representative blot is shown (bottom) demonstrating PKC- $\theta$  and SHP-1 expression. **(E)** WT YTS-2DL1, YTS-2DL1 SHP-1 KO, and YTS-2DL1 SHP-1 S591D NK cells were treated with PKC- $\theta$  or NS siRNA and were incubated with mCherry-expressing 721-Cw4 or 721-Cw7 target cells for 2 hr at 37°C and analyzed for degranulation via FACS. Degranulation was assessed relative to the WT

Figure 7 continued on next page

Figure 7 continued

NS-treated cells incubated with 721-Cw4 targets, as described in Materials and methods. For knockdown, cells were treated with either NS or PKC- $\theta$ -specific siRNA 24 hr before incubation with mCherry-expressing 721-Cw4 or 721-Cw7 target cells; the graph shows the average of four independent experiments. Data are shown as mean  $\pm$  SEM. Two-way ANOVA with Tukey test (**B, C**) or one-way ANOVA with Tukey test (**D, E**) was used to calculate p-values.

The online version of this article includes the following source data and figure supplement(s) for figure 7:

**Source data 1.** Numerical data for all the graphical presentations in **Figure 7**.

**Source data 2.** Representative blots.

**Figure supplement 1.** NK cell activation threshold is increased following gene silencing of PKC- $\theta$ .

**Figure supplement 1—source data 1.** Numerical data for the graphical presentation in **Figure 7—figure supplement 1**.

every 3 days for a total of six treatments (**Figure 8A**). Tumor volumes were monitored daily to examine the effect on tumor size and average growth rate (**Figure 8B–E**). If PKC- $\theta$  affects NK cell cytotoxicity through a dominant alternative pathway to SHP-1, then we would expect the observed phenotype of SHP-1 silenced/mutated NK cells (highly increased killing and arrest of tumor growth) to be abrogated, at least partially, upon PKC- $\theta$  silencing. Indeed, mice injected with YTS-2DL1 SHP-1-deficient/catalytically inactive cells that were treated with PKC- $\theta$  siRNA demonstrated slower tumor growth rates and smaller tumor volumes compared to mice injected with WT NK cells (**Figure 8**). In order to focus on the NK response toward targets cells that induce activating signals and demonstrate the involvement of PKC- $\theta$ -mediated SHP-1 phosphorylation in NK cell cytotoxicity, mice were subcutaneously engrafted with 721-Cw7 cells and injected as described above. As expected, PKC- $\theta$ -silenced NK cells exhibited decreased antitumor activity toward activating target cells (721-Cw7), while mice engrafted with YTS-2DL1 SHP-1 gene-silenced to PKC- $\theta$  exhibited a stronger antitumor response with lower tumor growth rates, suggesting that loss of SHP-1 activity restored the NK antitumor responses ( $p < 0.0001$ , **Figure 8D and E, Figure 8—figure supplement 1**). These results suggest that regulation of SHP-1 through PKC- $\theta$  impacts NK cell cytotoxicity and affects NK cell activity for in vivo tumor clearance.

## Discussion

SHP-1 plays a central role in the regulation of the NK cell activation threshold (**Stebbins et al., 2003; Lanier, 2005; Long, 2008; Matalon et al., 2016**) and is critical for the NK cell education process (**Viant et al., 2014**). Importantly, activation of SHP-1 and its homolog SHP-2 (an additional critical inhibitory NK cell regulatory enzyme) (**Purdy and Campbell, 2009**) are the major mechanisms operating downstream to immune checkpoint receptors, such as PD-1, CTLA-4, BTLA, and LAG-3 (**Lee et al., 1998; Watanabe et al., 2003; Sheppard et al., 2004; Huang et al., 2015**). It is therefore of great interest to understand how this important regulator is kept in check during NK cell activation and inhibition as this regulatory mechanism may have critical consequences for additional immune cells, immune checkpoint pathways, and immunotherapies.

NK cell activity is regulated by a balance between stimulatory or inhibitory signals, yet how these signals are integrated and how intracellular NK cell activation is maintained and controlled through these multiple receptors remain incompletely understood. Moreover, the presence of SHP-1 at the activating NKIS and rapid dispersal from the inhibitory NKIS (**Vyas et al., 2002a**) suggest as yet unknown roles and regulatory mechanisms. Here, we elucidate some of these unresolved mechanisms by showing that the NK cell activation threshold is maintained through downregulation of SHP-1 phosphatase activity regulated by PKC- $\theta$ .

Studies published on outcomes of SHP-1 C' terminal serine phosphorylation in non-NK cell systems demonstrated contradicting results (**Li et al., 1995; Brumell et al., 1997; Jones et al., 2004; Poole and Jones, 2005; Liu et al., 2007**). Here, we demonstrate that phosphorylation of SHP-1 by PKC- $\theta$  during NK cell activation on serine 591 maintains heightened NK cell effector function by retaining the SHP-1 closed and inactive conformation. This mechanism preserves SHP-1 substrate phosphorylation and consequently sustains calcium flux and cytotoxicity. Thus, the PKC- $\theta$ :SHP-1 axis may play an important role in NK immune surveillance and tumor clearance, a topic that has recently gained much attention in the immunotherapy field, especially in the context of adoptive cell transfer and genetically

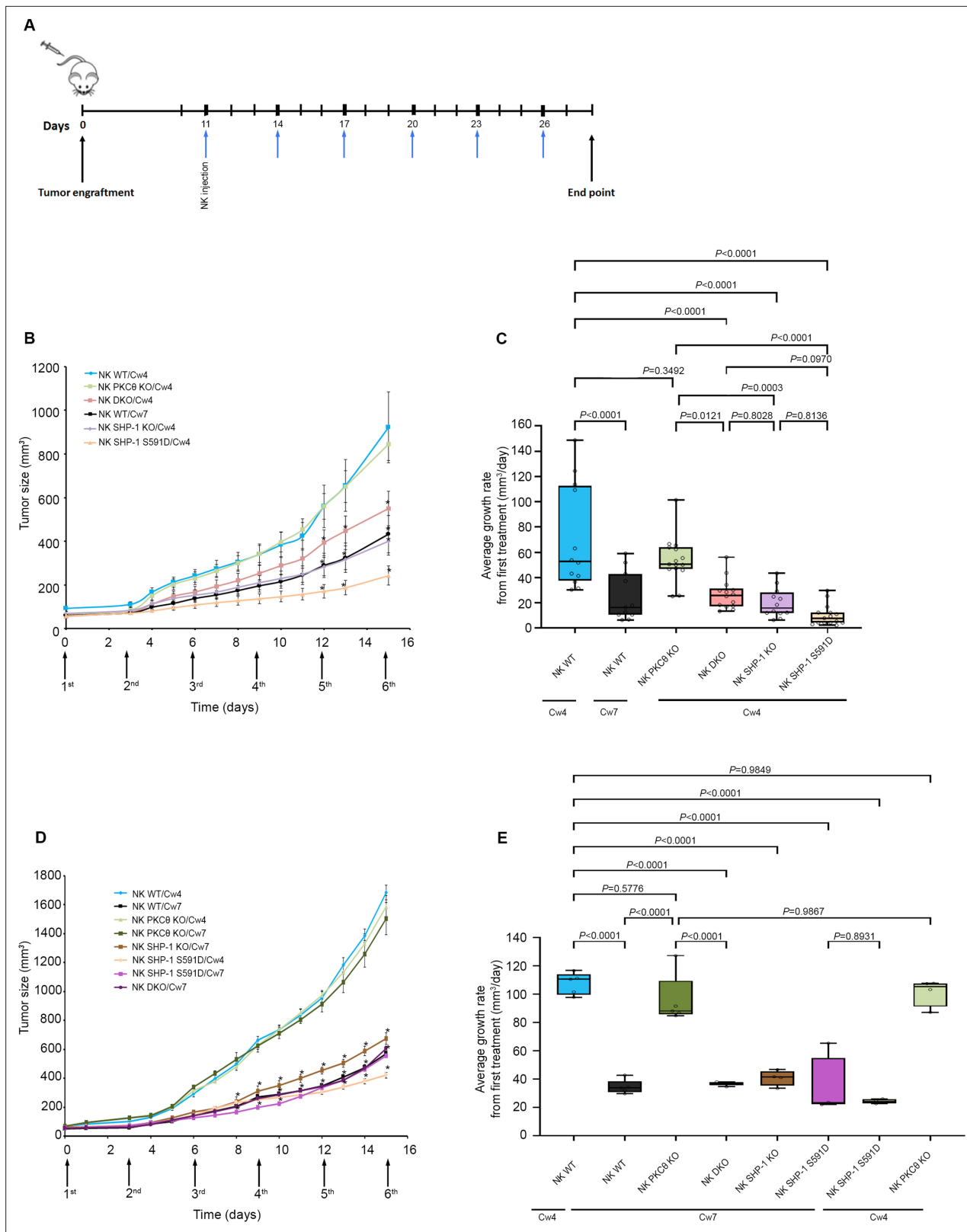


**Figure 8.** SHP-1-deficient NK cells exhibit enhanced antitumor activity in vivo, irrespective of PKC- $\theta$  expression. **(A)** Schematic representation of the experimental timeline. **(B)** Tumor volumes measured daily in NOD-Rag1<sup>null</sup>IL2r $\gamma$ <sup>null</sup> (RAG) mice. NOD-Rag1<sup>null</sup>IL2r $\gamma$ <sup>null</sup> (RAG) mice were subcutaneously injected with  $3 \times 10^6$  721-Cw4 or Cw7-expressing tumor cells. Mice were administered by intratumor injections every 3 days with either  $5 \times 10^6$  irradiated WT YTS-2DL1, WT YTS-2DL1 that were treated with PKC- $\theta$  siRNA (NK PKC- $\theta$  KO), YTS-2DL1 SHP-1 KO cells (NK SHP-1 KO), YTS-2DL1 SHP-1 KO cells

Figure 8 continued on next page



Figure 8 continued

that were treated with PKC- $\theta$  siRNA (NK DKO), or YTS-2DL1 SHP-1 S591D mutant cells. (C) Average growth rates of tumors from the first treatment to the end point. Tumor volumes and tumor growth rates were calculated as described in Materials and methods. Data are shown as mean  $\pm$  SEM. Two-way ANOVA with Tukey test (B, C) was used to calculate p-values. (D) Mice were subcutaneously injected with  $3 \times 10^6$  721-Cw4 or Cw7-expressing tumor cells. Mice were treated by intratumor injections every 3 days with either  $5 \times 10^6$  irradiated WT YTS-2DL1, WT YTS-2DL1 PKC- $\theta$  KO, YTS-2DL1 SHP-1 KO, YTS-2DL1 DKO, or YTS-2DL1 SHP-1 S591D mutant cells ( $n = 5$ ). Tumor volumes were measured daily. (E) Average growth rates of tumors from the first treatment to the end point. Tumor volumes and tumor growth rates were calculated as described in Materials and methods. Data are shown as mean  $\pm$  SEM. Two-way ANOVA with Tukey test (D, E) was used to calculate values.

The online version of this article includes the following source data and figure supplement(s) for figure 8:

**Source data 1.** Numerical data for all the graphical presentations in **Figure 8**.

**Figure supplement 1.** SHP-1-deficient natural killer (NK) cells exhibit decrease in the tumor volume, irrespective of PKC- $\theta$  expression.

engineered NK cells (Dotta et al., 2007; Morandi et al., 2008; Ahern and Brennan, 2011; Jochems et al., 2016; Siegler et al., 2017).

Our findings may answer an important question regarding how SHP-1 activity is downmodulated after dissociation of the inhibitory NKIS, and how its signaling is downregulated during cytolytic NK responses. Phosphorylation of SHP-1 during termination of the inhibitory NKIS may retain the activity of NK cells to subsequent targets, whereas its immediate phosphorylation at the activating NKIS maintains the NK cell lytic capacity. This is consistent with the SHP-1 conformation patterns shown here (Figure 2) within the activating and inhibitory NKIS.

Interestingly, mathematical modeling analysis in NK cells suggests that weak ligands for activating receptors (bearing partially phosphorylated ITAMs) can recruit SHP-1 and thereby increase the NK activation threshold, while under certain conditions (such as low concentration of SHP-1 and weak activating ligands) inhibitory receptors can aid in NK cell activation (Das, 2010). Thus, it is possible that one mechanism facilitating target cell escape from NK cell lysis is selection for cells expressing weak activating ligands that induce SHP-1 recruitment. It is clear that the transition of SHP-1 between inhibiting and activating receptors must be tightly regulated to ensure proper NK cell responses.

PKC- $\theta$  is the only PKC isoform that was shown to accumulate at T cell and NKISs (Monks et al., 1997; Merino et al., 2012). In T cells, it is clear that PKC- $\theta$  plays an important role in T cell activation and survival by activating several downstream pathways, including NF- $\kappa$ B and AP-1 as major targets (Wang et al., 2015). In addition, Merino et al. previously showed that clustering of PKC- $\theta$  at the NKIS amplifies murine NK cell activation and effector functions (Merino et al., 2012), but the mechanism by which it exerts this function and specifically in human cells remained mostly unknown. Several studies suggest the involvement of PKC- $\theta$  in signal transduction, antitumor activity, and NK cell degranulation (Anel et al., 2012). Here, we demonstrate that in human NK cells PKC- $\theta$  phosphorylates SHP-1 on S591 (Figure 4, Figure 3—figure supplement 1), suppresses SHP-1 activity, and thereby increases NK cell activity. PKC- $\theta$  appears to regulate SHP-1 activity during the late inhibitory synapse and through the full duration of activating NK:target cell interactions. Indeed, gene silencing of PKC- $\theta$  resulted in the closed SHP-1 conformation (Figure 5), implying that SHP-1 favors an open and active conformation in the absence of PKC- $\theta$ . This conformational change in SHP-1 also impacts its catalytic activity. These findings were strengthened through in vivo experiments, which demonstrated that absence of SHP-1 increased NK cell activity and decreased tumor progression, irrespective of PKC- $\theta$  expression, implying that PKC- $\theta$  indeed maintains NK cell activation through its regulation of SHP-1. PKC- $\theta$  also plays a role in NF- $\kappa$ B activation as shown by Sun et al., 2000. Thus, PKC- $\theta$  knockout could possibly affect NF- $\kappa$ B transcriptional activity, resulting in a reduced antitumor immune response. As shown in Figures 7E and 8D and E, YTS-2DL1 cells gene-silenced for PKC- $\theta$  show reduced degranulation, resulting in increased tumor growth rates, whereas YTS-2DL1 SHP-1 KO cells treated with PKC- $\theta$  siRNA (DKO) show increased degranulation and reduced tumor growth rate relative to YTS-2DL1 cells gene-silenced for PKC- $\theta$ , suggesting that SHP-1 knockout rescues the antitumor response. This result confirms the role of PKC- $\theta$  in regulating SHP-1 activity. It seems that a dynamic and coordinated balance between activating and inhibitory signaling cascades governs NK cell activation programs. Das et al. proposed that NK cell tolerance or activation is modulated by signal strength of the target cells (Das, 2010), which is in line with the suggestion that NK cell regulation occurs through a balance of activating and inhibitory signals transmitted by membrane receptors recognizing potential ligands on the target cell surface (Lanier, 2001). Here, we elucidate the potential circuitry between kinase and phosphatase activities playing a pivotal role in balancing activating

and inhibitory NK signaling. Several studies show that deficiency or inhibition of PKC- $\theta$  could potentially decrease the severity of autoimmunity, allergy, and chronic inflammation. For example, in animal models of intestinal inflammatory disease (chronic colitis), PKC- $\theta$  KO mice showed decreased T cell proliferation and cytokines production (*Chand et al., 2012; Curnock et al., 2014; Nicolle et al., 2021*), suggesting that PKC- $\theta$  inhibitors could be useful as a therapeutic approach for inflammatory disorders (*Chand et al., 2012; Curnock et al., 2014*).

Though pSHP-1 levels were substantially reduced after PKC- $\theta$  gene silencing, basal levels were still evident. It is possible that other serine/threonine kinases or isoforms such as PKC- $\theta$  may also be involved in this process (*Jones et al., 2004*). Another possible mechanism may involve PKC- $\theta$  cross talk with the NK cytoskeleton. We recently demonstrated that SHP-1 conformation and activity is dependent on the association to the cytoskeletal machinery and cytoskeletal dynamics (*Matalon et al., 2018*). One possibility is that cross-talk between PKC- $\theta$  and SHP-1 mediates actin:SHP-1 binding or disassociation, thereby regulating SHP-1 catalytic activity and conformation. Furthermore, PKC- $\theta$  phosphorylates the Wiskott-Interacting Protein (WIP) in NK cells upon activation, and this facilitates recruitment of actin and myosin IIA to WIP and WASp for the formation of the multiprotein complex (*Krzewski et al., 2006*).

After SHP-1 mediates its function and prevents NK cell activity during an inhibitory interaction, its activity should be downregulated to enable subsequent NK cell interactions with activating susceptible targets. This can be seen by late phosphorylation (after 20 min) of SHP-1 S591 during inhibitory NKISs (*Figure 1*), and may serve as a mechanism of kinetic priming, ensuring that NK cell activity remains stable for future contacts (*Choi and Mitchison, 2013*).

Recently, it was shown that as NK cells are constantly situated in an environment that requires simultaneous killing of target cells and sparing of others, accurate and specific convergence of lytic granules aids in killing only relevant targets, while sparing healthy cells (*Hsu et al., 2016*). Moreover, a study by Netter et al. demonstrated how initiation and termination of the activating NKIS are highly regulated and enable serial NK cell killing by accelerating detachment from one target cell and simultaneous formation of new cytotoxic NKISs (*Netter et al., 2017*). Additional reports by Srpan et al. describe NK cell serial killing via shedding of surface receptors (*Srpan et al., 2018*). Thus, sequential and highly regulated signaling is needed for NK cell maneuverability in a complex immune environment. PKC- $\theta$ : SHP1 regulation may enable an NK cell to rapidly survey its surroundings and maintain its effector functions in a complex immune environment that requires simultaneous sparing of normal cells and killing of malignant targets. This mechanism would also ensure that NK cell effector functions are maintained in the presence of an activating NKIS. Cancer cells can express MHC-I and other inhibitory NK cell ligands; thus, recruitment and activation of PKC- $\theta$  at the activating NKIS may limit SHP-1 association to ITIMs that could prevent tumor cell killing. It would be interesting to assess the effect of S591 phosphorylation on SHP-1:KIR ITIM association as this phosphorylation may not only affect the NK cell activation threshold, but also NK cell education, as SHP-1 was shown to be vital for regulating NK cell responsiveness to tumors (*Wu et al., 2021*).

Due to the fact that NK cells are also implicated in autoimmune disorders such as multiple sclerosis (*Morandi et al., 2008*), rheumatoid arthritis (*Ahern and Brennan, 2011*), and type I diabetes (*Dotta et al., 2007*), deregulation of SHP-1 activity may be a factor affecting normal NK cell functions against healthy cells. SHP-1 was also shown to serve as an important regulator that impacts cell proliferation and survival (*Chong and Maiese, 2007*). Some studies examined its role in tumor transformation (*Wu et al., 2003*). It would be interesting to examine whether mutations or regulation of SHP-1 S591 or other known or as yet unidentified residues may impact its function. Understanding regulatory protein circuits in NK cells will be an important step for further elucidating complex pathways such as NK signaling cascades and NK cell education, and potentially open doors to innovative immunotherapies shaping NK cell behavior.

## Materials and methods

### Key resources table

Reagent type (species) or resource	Designation	Source or reference	Identifiers	Additional information
Antibody	Anti-human PLC $\gamma$ 1 (mouse monoclonal)	Upstate	05-163	IB: 1:500 (14 $\mu$ L)

*Continued on next page*

Reagent type (species) or resource	Designation	Source or reference	Identifiers	Additional information
Antibody	Anti-human VAV1 (D7) (mouse monoclonal)	Santa Cruz	SC-8039	IB: 1:500 (14 $\mu$ L)
Antibody	Anti-human SHP-1 (SH-PTP-1) (C-19) (rabbit polyclonal)	Santa Cruz	SC-287	IB: 1:1000 (7 $\mu$ L)
Antibody	Anti-human GAPDH (0411) (mouse monoclonal)	Santa Cruz	SC-47724	IB: 1:1000 (7 $\mu$ L)
Antibody	Anti-human pSHP-1 (S591) (rabbit polyclonal)	ECM Biosciences	Sp-1531	IB: 1:1000 (7 $\mu$ L) IF: 1:500 (0.6 $\mu$ L)
Antibody	Anti-human pPLC $\gamma$ (Y783) (rabbit polyclonal)	Cell Signaling	CST-2821S	IB: 1:1000 (7 $\mu$ L) IF: 1:500 (0.6 $\mu$ L)
Antibody	Anti-human pVAV1 (Y160) (rabbit polyclonal)	Bio Source	Bs-44482	IB: 1:1000 (7 $\mu$ L) IF: 1:500 (0.6 $\mu$ L)
Antibody	Anti-human-PKC- $\theta$ (1C2) (mouse monoclonal)	Santa Cruz	SC-81534	IB: 1:500 (14 $\mu$ L) IF: 1:250 (1.2 $\mu$ L)
Antibody	Goat anti-mouse	Jackson Laboratory	#115-035-003	1:10,000 (1 $\mu$ L)
Antibody	Goat anti-rabbit	Santa Cruz	Sc-2004	1:10,000 (1 $\mu$ L)
Antibody	Anti-human KIR2DL1/S1-PE conjugated (mouse monoclonal)	Miltenyi Biotec	130-099-209	1:10 (10 $\mu$ L)
Antibody	Anti-human CD107a (LAMP-1) (mouse monoclonal)	BioLegend	#328602	1:20 (2.5 $\mu$ L)
Antibody	Alexa Fluor-conjugated 488 (goat polyclonal) anti-rabbit IgG (H+L) Highly Cross-Adsorbed Secondary Antibody	Invitrogen	A11034	IF: 1:2000 (1 $\mu$ L)
Antibody	Alexa Fluor-conjugated 488 goat polyclonal anti-mouse IgG (H+L)	Jackson Laboratory	115-545-146	IF: 1:2000 (1 $\mu$ L)
Recombinant DNA reagent	YFP-SHP-1-CFP (plasmid)	<b>Matalon et al., 2018</b>		
Recombinant DNA reagent	CRISPR CAS9 SHP-1 S591D	<b>Ben-Shmuel et al., 2021</b>		Backbone pSpCas9 (BB)-2A-GFP vector Addgene plasmid #48138
Sequence-based reagent	siRNA: target <i>PRKCQ</i> gene	Sigma-Aldrich		5' CUCUUCACCUAGGGCGCCAA 3' 5' UUGGCGCCAGGUGAAGAG 3'
Sequence-based reagent	siRNA: nonspecific target	Sigma-Aldrich		5' UAGCGACUAAACACAUCAA 3', 5'UAAGGCUAUGAAGAGAUAC3', 5'AUGUAUUGGCCUGUAUUAG3', 5' AUGAACGUGAAUUGCUCAA 3', and 5' UGGUUUACAUGUCGACUAA3'
Chemical compound, drug	Fluo-3-AM	Biotium	50016	1 $\mu$ g per sample
Chemical compound, drug	p-Nitrophenyl phosphate (pNPP)		NEB-P0757S	
Chemical compound, drug	[ <sup>35</sup> S]Met	PerkinElmer	NEG009L005MC	
Chemical compound, drug	Monensin	BioLegend	#420701	
Chemical reagent	Mirus	Ingenio Solution	MIR50111	
Chemical compound, reagent	Enhanced chemiluminescence	PerkinElmer, Life Gene	NEL105001EA, AC2103	

Reagent type (species) or resource	Designation	Source or reference	Identifiers	Additional information
chemical compound, reagent	Protein A/G plus-Agarose beads	Santa Cruz Biotechnology	SC-2003	
Commercial assay or kit	NK Cell enrichment kit	STEMCELL Technologies	Cat# 19055	
Commercial assay or kit	Human PE selection kit	STEMCELL Technologies	Cat# 18551	
Software, algorithm	GraphPad Prism	V9.0.1	RRID:SCR_002798	
Software, algorithm	Adobe Photoshop	CC2019		
Software, algorithm	FACS Diva			
Software, algorithm	ImageJ 1.53c	<a href="https://imagej.nih.gov/">https://imagej.nih.gov/</a>	RRID:SCR_003070	
Cell line ( <i>Homo sapiens</i> )	YTS KIR2DL1		RRID:CVCL_D324; parent: CVCL_1797 (YT); DSMZ no. ACC-434	Kind gift from Prof. Ofer Mandelboim STR profiling testing was done by DSMZ
Cell line ( <i>H. sapiens</i> )	721.221 HLA-Cw4		RRID:CVCL_6263; ATCC: CRL-1855	Kind gift from Prof. Ofer Mandelboim STR profiling was done by ATCC
Cell line ( <i>H. sapiens</i> )	721.221 HLA-Cw7		RRID:CVCL_6263; ATCC: CRL-1855	Kind gift from Prof. Ofer Mandelboim STR profiling was done by ATCC
Cell line ( <i>H. sapiens</i> )	K562		RRID:CVCL_0004; DSMZ no. ACC-434	Kind gift from Prof. Ofer Mandelboim STR profiling testing was done by DSMZ
Biological sample ( <i>H. sapiens</i> )	PBMCs			Blood samples from healthy donors were provided by Magen David Adom (MDA; Israeli National Blood Bank) Donor's identification information remained anonymous
Strain, strain background ( <i>Mus musculus</i> , female)	NOD-Rag1 <sup>null</sup> IL2rg <sup>null</sup> (RAG)	Jackson Labs	NOD-Rag1 <sup>null</sup> IL2rg <sup>null</sup> (RAG)	Details are listed in In vivo conditions and study design table
Strain, strain background ( <i>M. musculus</i> , female)	NOD-SCID IL2Rgamma <sup>null</sup> (NSG)	Jackson Labs	NOD-SCID IL2Rgamma <sup>null</sup> (NSG)	Details are listed in In vivo conditions and study design table

## Cell lines and reagents

The following cells were used in this study: YTS NK cell line expressing the inhibitory KIR2DL1 (referred as YTS-2DL1), B-cell lymphoma, 721.221 cells (referred as 721) expressing no HLA, and 721 cells expressing either HLA-Cw4 or -Cw7, and K562. These cells were kindly provided by Prof. Ofer Mandelboim (Department of Microbiology and Immunology, Faculty of Medicine, Hebrew University of Jerusalem, Israel). All the cell lines were tested negative for mycoplasma. YTS cells were cultured in Iscove's medium supplemented with 10% fetal bovine serum (FBS), 2 mM L-glutamine, 50 µg/mL penicillin, 50 µg/mL streptomycin, and 50 µM 2-mercapto-ethanol. 721.221 and K562 cells were cultured in RPMI supplemented with 10% FBS, 2 mM L-glutamine, 50 µg/mL penicillin, 50 µg/mL streptomycin, 1% non-essential amino acids, and 1% sodium pyruvate.

## Antibodies

Antibodies and their sources were as follows: mouse anti-PLCγ1 (Upstate), mouse anti-VAV1 (D7), rabbit anti-SHP-1 and mouse anti-GAPDH (Santa Cruz), rabbit anti-pSHP-1 (S591) (ECM Biosciences), rabbit anti-pPLCγ1Y783 (Bio Source), rabbit anti-pVAV-1Y160 (Bio Source), and mouse anti-PKC-θ (Santa Cruz). Secondary antibodies: goat anti-mouse (Sigma-Aldrich), goat anti-rabbit (Santa Cruz).

## Peripheral blood mononuclear cell (PBMC) isolation

Human primary PBMCs were isolated from whole blood of healthy donors, as previously described (*Barda-Saad et al., 2005*). Blood samples from anonymous healthy donors were provided by Magen David Adom (MDA; Israeli National Blood Bank). Informed consent was obtained from all donors. The experiments conformed to the principles set out in the WMA Declaration of Helsinki and the Department of Health and Human Services Belmont Report. The research was performed with approval of and according to the guidelines of the Bar-Ilan University Ethics Committee. Briefly, human PBMCs were isolated from whole blood by Ficoll-Histopaque density gradient centrifugation (MP Biomedical).

## Primary NK cells

Primary NK cells were isolated from PBMCs of healthy donors using the EasySep human NK Cell enrichment kit (STEMCELL Technologies). Subsequently, KIR2DL1-expressing cells were isolated by staining the entire NK cell population with anti-KIR2DL1/S1-PE antibody (Miltenyi Biotec) followed by magnetic separation using the EasySep human PE selection kit (STEMCELL Technologies) according to the manufacturer's instructions. NK cell isolation efficiencies were >95%. The NK cells were plated in 96-well U-bottomed plates and grown in the presence of irradiated PBLs from two donors ( $5 \times 10^4$  cells from each donor per well) as feeder cells. Cells were expanded in a complete medium containing 1  $\mu\text{g}/\text{mL}$  of PHA and 400 U/mL rhuIL-2 (ProSpec). Before experiments, cells were washed to remove the PHA and IL-2, and cultured 48 hr in 60% Dulbecco's modified Eagle's medium and 25% F-12 medium supplemented with 10% human serum, 2 mM L-glutamine, 50  $\mu\text{g}/\text{mL}$  penicillin, 50  $\mu\text{g}/\text{mL}$  streptomycin, 1% non-essential amino acids, and 1% sodium pyruvate.

## CRISPR/CAS9-mediated gene knockdown and S591D point mutation

CRISPR/CAS9 knockdown of *PTPN6* in YTS cells was conducted according to published protocol and was performed as described in detail (*Ran et al., 2013; Matalon et al., 2018*). The pSpCas9(B-B)-2A-GFP (PX458) vector was purchased from Addgene (plasmid# 48138). RNA guide sequences targeted to the SHP-1 locus and for knock-in of the S591D mutation were constructed using an online CRISPR design tool (Zhang Lab).

## RNA interference

siRNA to human 3' UTR *PRKCQ* was purchased from Sigma-Aldrich. YTS-2DL1 cells were transfected with siRNA specific for the indicated genes or NS siRNA as a control using an AMAXA electroporator.

For knockdown of *PRKCQ* gene expression, pools of independent specific siRNA oligonucleotides were as follows:

5' CUCUUCACCUUGGGCGCCAA 3'  
5' UUGGCGCCAGGUGAAGAG 3'

NS siRNA: Pools of nontargeting (nonspecific), negative control siRNA duplexes were obtained from Dharmacon with the following sequences: 5' UAGCGACUAAACACAUCAA 3', 5' UAAGGCUAUGAAGAGAUAC 3', 5' AUGUAUUGGCCUGUAUUAG 3', 5' AUGAACGUGAAUUGCUCAA 3', and 5' UGGUUUACAUGUCGACUAA 3'.

## Cellular imaging by confocal microscopy

Dynamic fluorescence and differential interference contrast (DIC) microscopy images of NK-target conjugates were collected using a Zeiss 510 Meta confocal microscope. All images were collected using a 63 $\times$  Plan-Apochromat objective (Carl Zeiss).

Chambered cover slips (LabTek) were cleaned by treatment with 1 M HCl, 70% ethanol for 30 min, and dried at 60°C for 30 min. The chambers were treated with a 0.01% (wt/vol) poly-L-lysine solution (Sigma) for 5 min, drained, and dried at 60°C for 30 min.

For NK-target conjugation assays,  $5 \times 10^5$  target cells were seeded over the bottom of the chamber in 300  $\mu\text{L}$  Optimem medium for 2 hr at 37°C, after which nonadherent cells were rinsed. Then,  $5 \times 10^5$  NK cells were seeded over the chambers, containing imaging buffer (RPMI medium with 25 mM HEPES without phenol red or serum), and allowed to form conjugates with the target cells for the indicated times at 37°C. Following activation, the cells were fixed for 30 min with 2.5% paraformaldehyde and washed twice with PBS. The NK and target cells in the conjugates were distinguished according

to fluorescence signal, with the target cells expressing mCherry. For evaluation of phosphoprotein accumulation at the NKIS, cells were permeabilized with 0.1% Triton X-100 for 5 min. Cells were then blocked for 1 hr in PFN buffer (PBS without  $\text{Ca}^{2+}$  and  $\text{Mg}^{2+}$  and containing 10% FBS and 0.02% azide) with 2% normal goat serum (Jackson ImmunoResearch). Cells were incubated for 1 hr with the appropriate primary antibodies diluted in blocking medium, followed by staining with isotype-specific, Alexa Fluor-conjugated antibodies for 30 min. Cells were washed three times with PFN between steps. The relative fluorescence intensities of the proteins at the NKIS were determined by measuring the ratio between the fluorescence intensity at the NKIS relative to that at a non-NKIS site using ImageJ software.

## Image processing and quantification

The acquired images were extracted with the LSM browser (Carl Zeiss), cropped, and composed into figures using Adobe Photoshop CC2019.

## FRET analysis

FRET was measured by the donor-sensitized acceptor fluorescence technique as previously described (*Barda-Saad et al., 2005; Pauker et al., 2012; Fried et al., 2014*). Briefly, three sets of filters were used: one optimized for donor fluorescence (excitation, 458 nm; emission, 465–510 nm), a second for acceptor fluorescence (excitation, 514 nm; emission, 530–600 nm), and a third for FRET (excitation, 458 nm; emission, 530–600 nm).

## FRET correction

FRET correction was performed as described in detail (*Barda-Saad et al., 2005; Pauker et al., 2012; Fried et al., 2014*). The non-FRET components were calculated and removed using calibration curves derived from images of single-labeled CFP- or YFP-expressing cells. Sets of reference images were obtained using the same acquisition parameters as those used for the experimental FRET images. To correct for CFP 'bleed through,' the intensity of each pixel in the CFP image from CFP-expressing cells was compared to the equivalent pixel in the FRET image of the same cells. A calibration curve was derived to define the level of CFP fluorescence seen in the FRET image as a function of the fluorescence in the CFP image. A similar calibration curve was obtained defining the amount of YFP fluorescence appearing in the FRET image as a function of the intensity in the YFP image using images of cells expressing only YFP. Separate calibration curves were derived for each set of acquisition parameters used in the FRET experiments. Then, using the appropriate calibration curves, together with the CFP and YFP images, the amount of CFP bleed through and YFP cross-excitation was calculated for each pixel in the experimental FRET images. These non-FRET components were subtracted from the raw FRET images, yielding corrected FRET images.

## FRET efficiency calculation

The FRET efficiency (FRET<sub>eff</sub>) was calculated on a pixel-by-pixel basis using the following equation:  $\text{FRET}_{\text{eff}} = \text{FRET}_{\text{corr}} / (\text{FRET}_{\text{corr}} + \text{CFP}) \times 100\%$ , where FRET<sub>corr</sub> is the pixel intensity in the corrected FRET image, and CFP is the intensity of the corresponding pixel in the CFP channel image.

To increase the reliability of the calculations and prevent low-level noise from distorting the calculated ratio, we excluded pixels below 50 intensity units and saturated pixels from the calculations and set their intensities to zero. These pixels are shown in black in the 'pseudocolored' FRET efficiency images.

To estimate the significance of the FRET efficiency values obtained and exclude the possibility of false-positive FRET results, we prepared cells expressing free CFP and free YFP as negative controls. The FRET efficiency in the negative control system was measured and calculated in the same way as in the main experiment. FRET efficiency values obtained from the negative control samples were subtracted from the values obtained in the main experiments. Image processing and measurements were performed using IPLab software version 3.9.

## PTP assay

SHP-1 catalytic activity was determined by measuring the hydrolysis of the exogenous substrate *p*-nitrophenyl phosphate (pNPP) by SHP-1, as previously described (*Lorenz, 2011; Matalon et al., 2018*).

NK cells ( $2\text{--}5 \times 10^6$ ) were incubated with target cells at a ratio of 1:1 at 37°C for 5 min before lysis. Cells were lysed with ice-cold passive lysis buffer (1.25% Brij, 0.625% *n*-octyl- $\beta$ -D-glucoside, 31.3 mM Tris-HCl, pH 7.4, 150 mM NaCl, 6.25 mM ethylenediaminetetraacetic acid, and cOmplete Protease Inhibitor Tablets [Roche]). Cell lysates were subjected to IP (immunoprecipitated) with anti-SHP-1 antibody. Immunoprecipitates were washed twice with ice-cold passive washing buffer (0.1% Brij, 50 mM Tris-HCl, pH 7.4, 300 mM NaCl, and 3.75 mM ethylenediaminetetraacetic acid), and three times with phosphatase buffer (150 mM NaCl, 50 mM HEPES, 10 mM ethylenediaminetetraacetic acid, and 1 mM DDT). Immunoprecipitates were resuspended in 200  $\mu$ L 25 mM pNPP in phosphatase buffer, and incubated for 30 min at 37°C. Reactions were terminated by adding 800  $\mu$ L 1 M NaOH, and SHP-1 activity was determined by measuring absorbance at 405 nm.

### Cytotoxicity assay

The cytolytic activity of NK cells against target cells was determined with a standard [ $^{35}$ S]Met release assay. Target cells were labeled with [ $^{35}$ S]Met (0.2 mCi/mL) for 12–16 hr and washed two times, and then  $5 \times 10^3$  cells were mixed with NK cells at an effector-to-target ratio of 10:1. Cells were then incubated for 5 hr at 37°C in complete medium. The cells were centrifuged at  $200 \times g$  for 5 min, the supernatant was mixed with scintillation liquid, and radioactive signal was measured with a  $\beta$  counter (Packard). Spontaneous release of [ $^{35}$ S]Met from an equal number of target cells was determined by adding 100 mL of complete medium to target cells that were incubated without NK cells. Maximal release was determined by adding 100 mL of 0.1 M NaOH to an equal number of target cells in the absence of NK cells. Finally, the percentage of cell lysis caused by the NK cells was calculated using the following equation: % specific lysis = [(sample signal – spontaneous release)/(maximal release – spontaneous release)]  $\times$  100.

### DNA constructs and mutagenesis

Human SHP-1 wt cDNA was obtained from Addgene. The cDNA of SHP-1 was subcloned into the expression vector pEYFP-N1 (Clontech) to obtain the chimeric protein YFP-SHP-1; pECFP-N1 (Clontech) was subcloned into the YFP-SHP-1 expression vector to obtain the chimeric protein YFP-SHP-1-CFP. To avoid localization of SHP-1 to the nucleus, YFP-SHP1-CFP was mutated at its NLS sequence (*He et al., 2005*). Molecular mutants were prepared using the QuikChange II XL site-directed mutagenesis kit (Stratagene). The mCherry plasmid was previously described (*Pauker et al., 2012*).

### Cell transfection and FACS analysis

YTS-2DL1 or 721.221/K562 cells were transfected with Nucleofector 2b (Lonza) using Amaxa solution R and protocol X-001. Transiently transfected cells were used after 24–48 hr. Cells transiently expressing chimeric proteins were selected in hygromycin. Fluorescence analysis and cell sorting were performed using FACSAria or FACSVantage (Becton Dickinson Biosciences).

### Cell stimulation, immunoblotting, and immunoprecipitation

First, NK cells (primary or YTS cell line) and 721.221 target cells (either expressing HLA-Cw4, Cw7, or no HLA) were incubated separately on ice for 10 min at a ratio of 1:1. The cells were mixed, centrifuged, and incubated on ice for 15 min. The cell mixture was then transferred to 37°C for the indicated period of time and subsequently lysed with ice-cold lysis buffer (1% Brij, 1% *n*-octyl- $\beta$ -D-glucoside, 50 mM Tris-HCl, pH 7.6, 150 mM NaCl, 5 mM ethylenediaminetetraacetic acid, 1 mM  $\text{Na}_3\text{VO}_4$ , and complete Protease Inhibitor Tablets [Roche]). YTS-2DL1 cells were incubated for 30 min on ice with the indicated concentration of pervanadate, before and at the time of NK-target cell co-culture.

For analysis of whole-cell lysates (WCL),  $1\text{--}5 \times 10^5$  cells were used, and for IP experiments  $10\text{--}15 \times 10^6$  cells were used. Protein A/G plus-Agarose beads (Santa Cruz Biotechnology) were used for IP. Protein samples were resolved with sodium dodecyl sulfate-polyacrylamide gel electrophoresis (SDS-PAGE), transferred to nitrocellulose membrane, and immunoblotted with the appropriate primary antibodies. Immunoreactive proteins were detected with either anti-mouse or anti-rabbit horseradish peroxidase-coupled secondary antibody followed by detection with enhanced chemiluminescence (PerkinElmer).

For WCL samples, the phosphorylation or expression level of proteins was measured by densitometric analysis relative to the GAPDH loading control using ImageJ. For IP samples, the relative

binding or phosphorylation level was measured by densitometric analysis relative to the precipitation control, using ImageJ.

### Measurement of intracellular calcium concentration

First,  $0.5\text{--}1 \times 10^6$  NK cells were incubated with  $1 \mu\text{g}$  calcium-sensitive dye, Fluo-3-AM per sample in (MPB) RPMI 1640 medium without phenol red, and containing 0.5 mM probenecid at  $37^\circ\text{C}$  for 45 min. The cells were washed once, resuspended in RPMI 1640 without phenol red containing 10 mM HEPES and 0.5 mM probenecid, and maintained at room temperature for 20 min. The cells were incubated at  $37^\circ\text{C}$  for 5 min before measurements, then mixed 1:1 with 721 target cells, and the  $\text{Ca}^{2+}$  influx was measured by spectrofluorimetry using the Synergy 4 Microplate Reader (BioTek).

### CD107a degranulation assay

NK cells ( $3 \times 10^5$ ) were co-incubated with  $6 \times 10^5$  target cells expressing mCherry at  $37^\circ\text{C}$  for 2 hr in the presence of  $2 \mu\text{M}$  monensin (BioLegend). The cells were centrifuged, incubated with 1:1000 diluted anti-CD107a for 30 min on ice, and washed twice. Cells were then stained with isotype-specific Alexa Fluor-conjugated antibody on ice for 30 min. Cells were washed twice and analyzed by FACS. YTS-2DL1 or pNK-2DL1 cells were distinguished from the target cells based on mCherry expression by the targets.

### Xenograft mice model

#### In vivo conditions and study design

Mouse model	Female SCID-NSG or SCID-NRG mice
Cell type and model	721.221-cw4 or cw7- B-NHL cell line Subcutaneous (SC)
Number of positions injected within the mouse body	1
Number of mice per cage	Five mice per cage
Irradiation	YTS cells were irradiated for a total of 200 cGy (no irradiation of mice)
Treatment: intratumor administration	100 $\mu\text{L}$ of $5 \times 10^6$ cells in PBS
Treatment injection interval	Every 3 days
Homing	SCID/NOD NSG or NRG female, 6–8-week-old mice were purchased from Envigo or Jackson laboratories. All mice were housed in IVC caging, supplied with irradiated shredded corn cob bedding and irradiated mouse feed diet. The light-dark cycle was 12 hr. The ambient temperature of each room was set at $20^\circ\text{C} \pm 1^\circ\text{C}$ . The temperature inside the boxes generally remained between $22^\circ\text{C}$ and $24^\circ\text{C}$ . Humidity was set between 35% and 55%.
Ethics oversight	Housing and breeding of mice and experimental procedures were performed according to the guidelines of the Bar-Ilan University Animal Ethics Committee (#82-10-18).
Study design	Randomization was used to divide the animals for in vivo treatments. No blinding was implemented as the researcher who performed the experiments also performed the analyses.

NOD-Rag1<sup>null</sup>IL2rg<sup>null</sup> (RAG) mice and NOD-SCID IL2Rgamma<sup>null</sup> (NSG) mice were purchased from the Jackson Labs. All mice used were from colonies that were inbred and maintained under SPF conditions at the Bar-Ilan animal house. Housing and breeding of mice and experimental procedures were performed according to the guidelines of the Bar-Ilan University Animal Ethics Committee, and 6–8-week old female RAG mice were subcutaneously injected, between the shoulders, with  $3 \times 10^6$  721-Cw4 or Cw7 HLA-expressing tumor cells, in 0.1 mL of PBS and Matrigel (Corning) (1:1 ratio). Mice were inspected daily for general well-being, and at the first indication of morbidity (weight loss,



lethargy, ruffled fur), or when they reached 8 weeks following inoculation, they were euthanized by CO<sub>2</sub>. Mice tumor diameters were measured daily with a digital caliper. Tumor volumes were calculated according to the formula:

$$\text{Tumor volume, (mm}^3\text{)} = (\text{smallest diameter}^2 \times \text{largest diameter}) / 2$$

When the tumor volumes reached 65–75 mm<sup>3</sup>, mice were intratumorally administered either 5 × 10<sup>6</sup> irradiated W.T YTS-2DL1 or SHP-1-KO NK cells that were untreated or treated with PKC-θ siRNA. Intratumor injections of NK cells were repeated every 3 days for six injections in total.

Average growth rates of the tumor from initiation of treatment were calculated according to the formula:

$$\text{Average growth rate} = (\text{Days of treatment}) / (\text{Last day tumor size} - \text{Initial tumor size})$$

## Statistical analyses

Data calculations of mean ± SEM were conducted in Microsoft Excel (v14.7.2), while data were graphed and statistical analysis was performed using GraphPad Prism 9.0.1 (GraphPad Software, Inc, USA). p-Values were calculated using a two-tailed unpaired t-test or one-sample t-test. Where more than two conditions were compared, a one-way ANOVA or two-way ANOVA with a Tukey post-test was used to calculate p-values. Data are depicted as columns with SE. Statistical parameters and biological replicates are reported in the figure legends.

## Acknowledgements

This research was partially funded by the United States–Israel Binational Science Foundation (2019211). The authors thank Danielle Keizer and Dr. Itay Lazar from Bar-Ilan University for their technical assistance. We also thank Dr. Michael Milyavsky and Dr. Adi Zipin-Roitman from Tel-Aviv university for generously providing the NOD-SCID IL2R<sup>γ</sup> null (NSG) mice, Dr. Jennifer Benichou Israel Cohen from Bar-Ilan University for her help with the statistical analysis, Dr. Liron Miller and Dr. Natalie Landa from the blood bank and transfusion center of Sheba medical center, Israel, for their technical assistance.

## Additional information

### Funding

Funder	Grant reference number	Author
Bar-Ilan University	United States–Israel Binational Science Foundation (2019211)	Mira Barda-Saad

The funders had no role in study design, data collection and interpretation, or the decision to submit the work for publication.

### Author contributions

Aviad Ben-Shmuel, Batel Sabag, Conceptualization, Data curation, Formal analysis, Investigation, Methodology, Software; Abhishek Puthenveetil, Moria Levy, Tammir Jubany, Jessica Kivelevitz, Data curation, Formal analysis; Guy Biber, Noah Joseph, Data curation, Formal analysis, Methodology; Fatima Awwad, Roshan Kumar Roy, Data curation; Omri Matalon, Conceptualization, Data curation, Formal analysis, Investigation, Methodology; Mira Barda-Saad, Conceptualization, Formal analysis, Funding acquisition, Investigation, Methodology, Project administration, Supervision, Validation, Visualization, Writing - original draft, Writing - review and editing

### Author ORCIDs

Aviad Ben-Shmuel  <http://orcid.org/0000-0002-5115-9922>  
 Batel Sabag  <http://orcid.org/0000-0002-3003-8080>

Abhishek Puthenveetil  <http://orcid.org/0000-0002-6310-3328>

Tammir Jubany  <http://orcid.org/0000-0001-9736-5062>

Mira Barda-Saad  <http://orcid.org/0000-0002-0305-7438>

### Ethics

Blood samples from healthy donors were randomly collected and provided by Magen David Adom. No patient's identification information was provided. The research was performed according to ethical principles for medical research involving human subjects.

Housing and breeding of mice and experimental procedures were performed according to the guidelines of the Bar-Ilan University Ethics committee.

### Decision letter and Author response

Decision letter <https://doi.org/10.7554/eLife.73282.sa1>

Author response <https://doi.org/10.7554/eLife.73282.sa2>

---

## Additional files

### Supplementary files

- Transparent reporting form

### Data availability

Source data files for numerical data and representative blots are now provided for figures and figure supplements.

## References

- Aguiló JI**, Garaude J, Pardo J, Villalba M, Anel A. 2009. Protein kinase C-theta is required for NK cell activation and in vivo control of tumor progression. *Journal of Immunology (Baltimore, Md)* **182**:1972–1981. DOI: <https://doi.org/10.4049/jimmunol.0801820>, PMID: 19201850
- Ahern DJ**, Brennan FM. 2011. The role of Natural Killer cells in the pathogenesis of rheumatoid arthritis: major contributors or essential homeostatic modulators? *Immunology Letters* **136**:115–121. DOI: <https://doi.org/10.1016/j.imlet.2010.11.001>, PMID: 21073898
- André P**, Castriconi R, Espéli M, Anfossi N, Juarez T, Hue S, Conway H, Romagné F, Dondero A, Nanni M, Caillat-Zucman S, Raulet DH, Bottino C, Vivier E, Moretta A, Paul P. 2004. Comparative analysis of human NK cell activation induced by NKG2D and natural cytotoxicity receptors. *European Journal of Immunology* **34**:961–971. DOI: <https://doi.org/10.1002/eji.200324705>, PMID: 15048706
- Andzelm MM**, Chen X, Krzewski K, Orange JS, Strominger JL. 2007. Myosin IIA is required for cytolytic granule exocytosis in human NK cells. *The Journal of Experimental Medicine* **204**:2285–2291. DOI: <https://doi.org/10.1084/jem.20071143>, PMID: 17875677
- Anel A**, Aguiló JI, Catalán E, Garaude J, Rathore MG, Pardo J, Villalba M. 2012. Protein Kinase C-θ (PKC-θ) in Natural Killer Cell Function and Anti-Tumor Immunity. *Frontiers in Immunology* **3**:187. DOI: <https://doi.org/10.3389/fimmu.2012.00187>, PMID: 22783260
- Baier G**, Telford D, Giampa L, Coggeshall KM, Baier-Bitterlich G, Isakov N, Altman A. 1993. Molecular cloning and characterization of PKC theta, a novel member of the protein kinase C (PKC) gene family expressed predominantly in hematopoietic cells. *The Journal of Biological Chemistry* **268**:4997–5004. DOI: [https://doi.org/10.1016/S0021-9258\(18\)53494-3](https://doi.org/10.1016/S0021-9258(18)53494-3), PMID: 8444877
- Barda-Saad M**, Braiman A, Titerence R, Bunnell SC, Barr VA, Samelson LE. 2005. Dynamic molecular interactions linking the T cell antigen receptor to the actin cytoskeleton. *Nature Immunology* **6**:80–89. DOI: <https://doi.org/10.1038/ni1143>, PMID: 15558067
- Ben-Shmuel A**, Biber G, Sabag B, Barda-Saad M. 2021. Modulation of the intracellular inhibitory checkpoint SHP-1 enhances the antitumor activity of engineered NK cells. *Cellular & Molecular Immunology* **18**:1314–1316. DOI: <https://doi.org/10.1038/s41423-020-0443-6>, PMID: 32341521
- Brumell JH**, Chan CK, Butler J, Borregaard N, Siminovitch KA, Grinstein S, Downey GP. 1997. Regulation of Src homology 2-containing tyrosine phosphatase 1 during activation of human neutrophils. Role of protein kinase C. *The Journal of Biological Chemistry* **272**:875–882. DOI: <https://doi.org/10.1074/jbc.272.2.875>, PMID: 8995376
- Bryceson YT**, March ME, Ljunggren HG, Long EO. 2006. Synergy among receptors on resting NK cells for the activation of natural cytotoxicity and cytokine secretion. *Blood* **107**:159–166. DOI: <https://doi.org/10.1182/blood-2005-04-1351>, PMID: 16150947
- Burroughs NJ**, Wülfing C. 2002. Differential segregation in a cell-cell contact interface: the dynamics of the immunological synapse. *Biophysical Journal* **83**:1784–1796. DOI: [https://doi.org/10.1016/S0006-3495\(02\)73944-1](https://doi.org/10.1016/S0006-3495(02)73944-1), PMID: 12324401

- Caraux A**, Kim N, Bell SE, Zompi S, Ranson T, Lesjean-Pottier S, Garcia-Ojeda ME, Turner M, Colucci F. 2006. Phospholipase C-gamma2 is essential for NK cell cytotoxicity and innate immunity to malignant and virally infected cells. *Blood* **107**:994–1002. DOI: <https://doi.org/10.1182/blood-2005-06-2428>, PMID: 16204312
- Carisey AF**, Mace EM, Saeed MB, Davis DM, Orange JS. 2018. Nanoscale Dynamism of Actin Enables Secretory Function in Cytolytic Cells. *Current Biology* **28**:489–502. DOI: <https://doi.org/10.1016/j.cub.2017.12.044>, PMID: 29398219
- Carretero M**, Palmieri G, Llano M, Tullio V, Santoni A, Geraghty DE, López-Botet M. 1998. Specific engagement of the CD94/NKG2-A killer inhibitory receptor by the HLA-E class Ib molecule induces SHP-1 phosphatase recruitment to tyrosine-phosphorylated NKG2-A: evidence for receptor function in heterologous transfectants. *European Journal of Immunology* **28**:1280–1291. DOI: [https://doi.org/10.1002/\(SICI\)1521-4141\(199804\)28:04<1280::AID-IMMU1280>3.0.CO;2-O](https://doi.org/10.1002/(SICI)1521-4141(199804)28:04<1280::AID-IMMU1280>3.0.CO;2-O), PMID: 9565368
- Chand S**, Mehta N, Bahia MS, Dixit A, Silakari O. 2012. Protein kinase C-theta inhibitors: A novel therapy for inflammatory disorders. *Current Pharmaceutical Design* **18**:4725–4746. DOI: <https://doi.org/10.2174/138161212802651625>, PMID: 22830352
- Chemnitz JM**, Parry RV, Nichols KE, June CH, Riley JL. 2004. SHP-1 and SHP-2 associate with immunoreceptor tyrosine-based switch motif of programmed death 1 upon primary human T cell stimulation, but only receptor ligation prevents T cell activation. *Journal of Immunology (Baltimore, Md)* **173**:945–954. DOI: <https://doi.org/10.4049/jimmunol.173.2.945>, PMID: 15240681
- Choi PJ**, Mitchison TJ. 2013. Imaging burst kinetics and spatial coordination during serial killing by single natural killer cells. *PNAS* **110**:6488–6493. DOI: <https://doi.org/10.1073/pnas.1221312110>, PMID: 23576740
- Chong ZZ**, Maiese K. 2007. The Src homology 2 domain tyrosine phosphatases SHP-1 and SHP-2: diversified control of cell growth, inflammation, and injury. *Histology and Histopathology* **22**:1251–1267.
- Curnock A**, Bolton C, Chiu P, Doyle E, Frayse D, Hesse M, Jones J, Weber P, Jimenez JM. 2014. Selective protein kinase C $\theta$  (PKC $\theta$ ) inhibitors for the treatment of autoimmune diseases. *Biochemical Society Transactions* **42**:1524–1528. DOI: <https://doi.org/10.1042/BST20140167>, PMID: 25399564
- Das J**. 2010. Activation or tolerance of natural killer cells is modulated by ligand control in a nonmonotonic manner. *Biophysical Journal* **99**:2028–2037. DOI: <https://doi.org/10.1016/j.bpj.2010.07.061>, PMID: 20923636
- Dong Z**, Davidson D, Pérez-Quintero LA, Kurosaki T, Swat W, Veillette A. 2012. The adaptor SAP controls NK cell activation by regulating the enzymes Vav-1 and SHIP-1 and by enhancing conjugates with target cells. *Immunity* **36**:974–985. DOI: <https://doi.org/10.1016/j.immuni.2012.03.023>, PMID: 22683124
- Dotta F**, Censini S, van Halteren AGS, Marselli L, Masini M, Dionisi S, Mosca F, Boggi U, Muda AO, Del Prato S, Elliott JF, Covacci A, Rappuoli R, Roep BO, Marchetti P. 2007. Coxsackie B4 virus infection of beta cells and natural killer cell insulinitis in recent-onset type 1 diabetic patients. *PNAS* **104**:5115–5120. DOI: <https://doi.org/10.1073/pnas.0700442104>, PMID: 17360338
- Egelhoff TT**, Lee RJ, Spudich JA. 1993. *Dictyostelium* myosin heavy chain phosphorylation sites regulate myosin filament assembly and localization in vivo. *Cell* **75**:363–371. DOI: [https://doi.org/10.1016/0092-8674\(93\)80077-r](https://doi.org/10.1016/0092-8674(93)80077-r), PMID: 7691416
- Feng J**, Garrity D, Call ME, Moffett H, Wucherpfennig KW. 2005. Convergence on a distinctive assembly mechanism by unrelated families of activating immune receptors. *Immunity* **22**:427–438. DOI: <https://doi.org/10.1016/j.immuni.2005.02.005>, PMID: 15845448
- Forslund E**, Sohlberg E, Enqvist M, Olofsson PE, Malmberg K-J, Önfelt B. 2015. Microchip-Based Single-Cell Imaging Reveals That CD56dimCD57-KIR-NKG2A+ NK Cells Have More Dynamic Migration Associated with Increased Target Cell Conjugation and Probability of Killing Compared to CD56dimCD57-KIR-NKG2A- NK Cells. *Journal of Immunology (Baltimore, Md)* **195**:3374–3381. DOI: <https://doi.org/10.4049/jimmunol.1500171>, PMID: 26320254
- Fried S**, Reicher B, Pauker MH, Eliyahu S, Matalon O, Noy E, Chill J, Barda-Saad M. 2014. Triple-color FRET analysis reveals conformational changes in the WIP-WASp actin-regulating complex. *Science Signaling* **7**:ra60. DOI: <https://doi.org/10.1126/scisignal.2005198>, PMID: 24962707
- Guldevall K**, Brandt L, Forslund E, Olofsson K, Frisk TW, Olofsson PE, Gustafsson K, Manneberg O, Vanherberghen B, Brismar H, Kärre K, Uhlin M, Önfelt B. 2016. Microchip Screening Platform for Single Cell Assessment of NK Cell Cytotoxicity. *Frontiers in Immunology* **7**:119. DOI: <https://doi.org/10.3389/fimmu.2016.00119>, PMID: 27092139
- Hayashi K**, Altman A. 2007. Protein kinase C theta (PKCtheta): a key player in T cell life and death. *Pharmacological Research* **55**:537–544. DOI: <https://doi.org/10.1016/j.phrs.2007.04.009>, PMID: 17544292
- He D**, Song X, Liu L, Burk DH, Zhou GW. 2005. EGF-stimulation activates the nuclear localization signal of SHP-1. *Journal of Cellular Biochemistry* **94**:944–953. DOI: <https://doi.org/10.1002/jcb.20307>, PMID: 15578567
- Hsu HT**, Mace EM, Carisey AF, Viswanath DI, Christakou AE, Wiklund M, Önfelt B, Orange JS. 2016. NK cells converge lytic granules to promote cytotoxicity and prevent bystander killing. *The Journal of Cell Biology* **215**:875–889. DOI: <https://doi.org/10.1083/jcb.201604136>, PMID: 27903610
- Huang W**, Erikson RL. 1994. Constitutive activation of Mek1 by mutation of serine phosphorylation sites. *PNAS* **91**:8960–8963. DOI: <https://doi.org/10.1073/pnas.91.19.8960>, PMID: 8090753
- Huang RY**, Eppolito C, Lele S, Shrikant P, Matsuzaki J, Odunsi K. 2015. LAG3 and PD1 co-inhibitory molecules collaborate to limit CD8+ T cell signaling and dampen antitumor immunity in a murine ovarian cancer model. *Oncotarget* **6**:27359–27377. DOI: <https://doi.org/10.18632/oncotarget.4751>, PMID: 26318293
- Jochems C**, Hodge JW, Fantini M, Fujii R, Morillon YM, Greiner JW, Padgett MR, Tritsch SR, Tsang KY, Campbell KS, Klingemann H, Boissel L, Rabizadeh S, Soon-Shiong P, Schlom J. 2016. An NK cell line (haNK)

- expressing high levels of granzyme and engineered to express the high affinity CD16 allele. *Oncotarget* **7**:86359–86373. DOI: <https://doi.org/10.18632/oncotarget.13411>, PMID: 27861156
- Jones ML**, Craik JD, Gibbins JM, Poole AW. 2004. Regulation of SHP-1 tyrosine phosphatase in human platelets by serine phosphorylation at its C terminus. *The Journal of Biological Chemistry* **279**:40475–40483. DOI: <https://doi.org/10.1074/jbc.M402970200>, PMID: 15269224
- Kim HS**, Das A, Gross CC, Bryceson YT, Long EO. 2010. Synergistic signals for natural cytotoxicity are required to overcome inhibition by c-Cbl ubiquitin ligase. *Immunity* **32**:175–186. DOI: <https://doi.org/10.1016/j.immuni.2010.02.004>, PMID: 20189481
- Krzewski K**, Chen X, Orange JS, Strominger JL. 2006. Formation of a WIP-, WASp-, actin-, and myosin IIA-containing multiprotein complex in activated NK cells and its alteration by KIR inhibitory signaling. *The Journal of Cell Biology* **173**:121–132. DOI: <https://doi.org/10.1083/jcb.200509076>, PMID: 16606694
- Lanier LL**. 2001. On guard--activating NK cell receptors. *Nature Immunology* **2**:23–27. DOI: <https://doi.org/10.1038/83130>, PMID: 11135574
- Lanier LL**. 2003. Natural killer cell receptor signaling. *Current Opinion in Immunology* **15**:308–314. DOI: [https://doi.org/10.1016/s0952-7915\(03\)00039-6](https://doi.org/10.1016/s0952-7915(03)00039-6), PMID: 12787756
- Lanier LL**. 2005. NK cell recognition. *Annual Review of Immunology* **23**:225–274. DOI: <https://doi.org/10.1146/annurev.immunol.23.021704.115526>, PMID: 15771571
- Lee KM**, Chuang E, Griffin M, Khattri R, Hong DK, Zhang W, Straus D, Samelson LE, Thompson CB, Bluestone JA. 1998. Molecular basis of T cell inactivation by CTLA-4. *Science (New York, N.Y.)* **282**:2263–2266. DOI: <https://doi.org/10.1126/science.282.5397.2263>, PMID: 9856951
- Léger J**, Kempf M, Lee G, Brandt R. 1997. Conversion of serine to aspartate imitates phosphorylation-induced changes in the structure and function of microtubule-associated protein tau. *The Journal of Biological Chemistry* **272**:8441–8446. DOI: <https://doi.org/10.1074/jbc.272.13.8441>, PMID: 9079670
- Li RY**, Gaits F, Ragab A, Ragab-Thomas JM, Chap H. 1995. Tyrosine phosphorylation of an SH2-containing protein tyrosine phosphatase is coupled to platelet thrombin receptor via a pertussis toxin-sensitive heterotrimeric G-protein. *The EMBO Journal* **14**:2519–2526. DOI: <https://doi.org/10.1002/j.1460-2075.1995.tb07249.x>
- Liu Y**, Kruhlak MJ, Hao JJ, Shaw S. 2007. Rapid T cell receptor-mediated SHP-1 S591 phosphorylation regulates SHP-1 cellular localization and phosphatase activity. *Journal of Leukocyte Biology* **82**:742–751. DOI: <https://doi.org/10.1189/jlb.1206736>, PMID: 17575265
- Long EO**. 2008. Negative signaling by inhibitory receptors: the NK cell paradigm. *Immunological Reviews* **224**:70–84. DOI: <https://doi.org/10.1111/j.1600-065X.2008.00660.x>, PMID: 18759921
- Lorenz U**. 2009. SHP-1 and SHP-2 in T cells: two phosphatases functioning at many levels. *Immunological Reviews* **228**:342–359. DOI: <https://doi.org/10.1111/j.1600-065X.2008.00760.x>, PMID: 19290938
- Lorenz U**. 2011. Protein tyrosine phosphatase assays. *Current Protocols in Immunology* **Chapter 11**:im1107s93. DOI: <https://doi.org/10.1002/0471142735.im1107s93>, PMID: 21462163
- Malhotra A**, Shanker A. 2011. NK cells: immune cross-talk and therapeutic implications. *Immunotherapy* **3**:1143–1166. DOI: <https://doi.org/10.2217/imt.11.102>, PMID: 21995569
- Matalon O**, Fried S, Ben-Shmuel A, Pauker MH, Joseph N, Keizer D, Piterburg M, Barda-Saad M. 2016. Dephosphorylation of the adaptor LAT and phospholipase C-γ by SHP-1 inhibits natural killer cell cytotoxicity. *Science Signaling* **9**:1–16. DOI: <https://doi.org/10.1126/scisignal.aad6182>, PMID: 27221712
- Matalon O**, Ben-Shmuel A, Kivelevitz J, Sabag B, Fried S, Joseph N, Noy E, Biber G, Barda-Saad M. 2018. Actin retrograde flow controls natural killer cell response by regulating the conformation state of SHP-1. *The EMBO Journal* **37**:e96264. DOI: <https://doi.org/10.15252/embj.201696264>, PMID: 29449322
- Merino E**, Abeyweera TP, Firth MA, Zawislak CL, Basu R, Liu X, Sun JC, Huse M. 2012. Protein kinase C-θ clustering at immunological synapses amplifies effector responses in NK cells. *Journal of Immunology (Baltimore, Md)* **189**:4859–4869. DOI: <https://doi.org/10.4049/jimmunol.1200825>, PMID: 23077238
- Mizesko MC**, Banerjee PP, Monaco-Shawver L, Mace EM, Bernal WE, Sawalle-Belohradsky J, Belohradsky BH, Heinz V, Freeman AF, Sullivan KE, Holland SM, Torgerson TR, Al-Herz W, Chou J, Hanson IC, Albert MH, Geha RS, Renner ED, Orange JS. 2013. Defective actin accumulation impairs human natural killer cell function in patients with dedicator of cytokinesis 8 deficiency. *The Journal of Allergy and Clinical Immunology* **131**:840–848. DOI: <https://doi.org/10.1016/j.jaci.2012.12.1568>, PMID: 23380217
- Monks CR**, Kupfer H, Tamir I, Barlow A, Kupfer A. 1997. Selective modulation of protein kinase C-θ during T-cell activation. *Nature* **385**:83–86. DOI: <https://doi.org/10.1038/385083a0>, PMID: 8985252
- Morandi B**, Bramanti P, Bonaccorsi I, Montalto E, Oliveri D, Pezzino G, Navarra M, Ferlazzo G. 2008. Role of natural killer cells in the pathogenesis and progression of multiple sclerosis. *Pharmacological Research* **57**:1–5. DOI: <https://doi.org/10.1016/j.phrs.2007.11.003>, PMID: 18182304
- Moretta L**, Ciccone E, Mingari MC, Biassoni R, Moretta A. 1994. Human natural killer cells: origin, clonality, specificity, and receptors. *Advances in Immunology* **55**:341–380. DOI: [https://doi.org/10.1016/s0065-2776\(08\)60513-1](https://doi.org/10.1016/s0065-2776(08)60513-1), PMID: 7508176
- Münz C**, Holmes N, King A, Loke YW, Colonna M, Schild H, Rammensee HG. 1997. Human histocompatibility leukocyte antigen (HLA)-G molecules inhibit NKAT3 expressing natural killer cells. *The Journal of Experimental Medicine* **185**:385–391. DOI: <https://doi.org/10.1084/jem.185.3.385>, PMID: 9053439
- Netter P**, Anft M, Watzl C. 2017. Termination of the Activating NK Cell Immunological Synapse Is an Active and Regulated Process. *Journal of Immunology (Baltimore, Md)* **199**:2528–2535. DOI: <https://doi.org/10.4049/jimmunol.1700394>, PMID: 28835459

- Nicolle A**, Zhang Y, Belguise K. 2021. The Emerging Function of PKC $\theta$  in Cancer. *Biomolecules* **11**:1–12. DOI: <https://doi.org/10.3390/biom11020221>, PMID: 33562506
- Orange JS**, Ramesh N, Remold-O'Donnell E, Sasahara Y, Koopman L, Byrne M, Bonilla FA, Rosen FS, Geha RS, Strominger JL. 2002. Wiskott-Aldrich syndrome protein is required for NK cell cytotoxicity and colocalizes with actin to NK cell-activating immunologic synapses. *PNAS* **99**:11351–11356. DOI: <https://doi.org/10.1073/pnas.162376099>, PMID: 12177428
- Orr MT**, Lanier LL. 2010. Natural killer cell education and tolerance. *Cell* **142**:847–856. DOI: <https://doi.org/10.1016/j.cell.2010.08.031>, PMID: 20850008
- Osada S**, Mizuno K, Saido TC, Suzuki K, Kuroki T, Ohno S. 1992. A new member of the protein kinase C family, nPKC $\theta$ , predominantly expressed in skeletal muscle. *Molecular and Cellular Biology* **12**:3930–3938. DOI: <https://doi.org/10.1128/mcb.12.9.3930-3938.1992>, PMID: 1508194
- Page KM**, Chaudhary D, Goldman SJ, Kasaian MT. 2008. Natural killer cells from protein kinase C $\theta$ -/- mice stimulated with interleukin-12 are deficient in production of interferon- $\gamma$ . *Journal of Leukocyte Biology* **83**:1267–1276. DOI: <https://doi.org/10.1189/jlb.1107745>, PMID: 18263766
- Pauker MH**, Hassan N, Noy E, Reicher B, Barda-Saad M. 2012. Studying the dynamics of SLP-76, Nck, and Vav1 multimolecular complex formation in live human cells with triple-color FRET. *Science Signaling* **5**:rs3. DOI: <https://doi.org/10.1126/scisignal.2002423>, PMID: 22534133
- Pipkin ME**, Lieberman J. 2007. Delivering the kiss of death: progress on understanding how perforin works. *Current Opinion in Immunology* **19**:301–308. DOI: <https://doi.org/10.1016/j.coi.2007.04.011>, PMID: 17433871
- Poole AW**, Jones ML. 2005. A SHPing tale: perspectives on the regulation of SHP-1 and SHP-2 tyrosine phosphatases by the C-terminal tail. *Cellular Signalling* **17**:1323–1332. DOI: <https://doi.org/10.1016/j.cellsig.2005.05.016>, PMID: 16084691
- Purdy AK**, Campbell KS. 2009. SHP-2 expression negatively regulates NK cell function. *Journal of Immunology (Baltimore, Md)* **183**:7234–7243. DOI: <https://doi.org/10.4049/jimmunol.0900088>, PMID: 19915046
- Ran FA**, Hsu PD, Wright J, Agarwala V, Scott DA, Zhang F. 2013. Genome engineering using the CRISPR-Cas9 system. *Nature Protocols* **8**:2281–2308. DOI: <https://doi.org/10.1038/nprot.2013.143>, PMID: 24157548
- Sheppard K-A**, Fitz LJ, Lee JM, Benander C, George JA, Wooters J, Qiu Y, Jussif JM, Carter LL, Wood CR, Chaudhary D. 2004. PD-1 inhibits T-cell receptor induced phosphorylation of the ZAP70/CD3zeta signalosome and downstream signaling to PKC $\theta$ . *FEBS Letters* **574**:37–41. DOI: <https://doi.org/10.1016/j.febslet.2004.07.083>, PMID: 15358536
- Siegler EL**, Kim YJ, Chen X, Siritwon N, Mac J, Rohrs JA, Bryson PD, Wang P. 2017. Combination Cancer Therapy Using Chimeric Antigen Receptor-Engineered Natural Killer Cells as Drug Carriers. *Molecular Therapy* **25**:2607–2619. DOI: <https://doi.org/10.1016/j.ymthe.2017.08.010>, PMID: 28919377
- Srpan K**, Ambrose A, Karampatzakis A, Saeed M, Cartwright ANR, Guldevall K, De Matos GDSC, Önfelt B, Davis DM. 2018. Shedding of CD16 disassembles the NK cell immune synapse and boosts serial engagement of target cells. *The Journal of Cell Biology* **217**:3267–3283. DOI: <https://doi.org/10.1083/jcb.201712085>, PMID: 29967280
- Stebbins CC**, Watzl C, Billadeau DD, Leibson PJ, Burshtyn DN, Long EO. 2003. Vav1 dephosphorylation by the tyrosine phosphatase SHP-1 as a mechanism for inhibition of cellular cytotoxicity. *Molecular and Cellular Biology* **23**:6291–6299. DOI: <https://doi.org/10.1128/MCB.23.17.6291-6299.2003>, PMID: 12917349
- Sun Z**, Arendt CW, Ellmeier W, Schaeffer EM, Sunshine MJ, Gandhi L, Annes J, Petrzilka D, Kupfer A, Schwartzberg PL, Littman DR. 2000. PKC- $\theta$  is required for TCR-induced NF- $\kappa$ B activation in mature but not immature T lymphocytes. *Nature* **404**:402–407. DOI: <https://doi.org/10.1038/35006090>, PMID: 10746729
- Tassi I**, Cella M, Presti R, Colucci A, Gilfillan S, Littman DR, Colonna M. 2008. NK cell-activating receptors require PKC- $\theta$  for sustained signaling, transcriptional activation, and IFN- $\gamma$  secretion. *Blood* **112**:4109–4116. DOI: <https://doi.org/10.1182/blood-2008-02-139527>, PMID: 18784374
- Topham NJ**, Hewitt EW. 2009. Natural killer cell cytotoxicity: how do they pull the trigger? *Immunology* **128**:7–15. DOI: <https://doi.org/10.1111/j.1365-2567.2009.03123.x>, PMID: 19689731
- Upshaw JL**, Arneson LN, Schoon RA, Dick CJ, Billadeau DD, Leibson PJ. 2006. NKG2D-mediated signaling requires a DAP10-bound Grb2-Vav1 intermediate and phosphatidylinositol-3-kinase in human natural killer cells. *Nature Immunology* **7**:524–532. DOI: <https://doi.org/10.1038/ni1325>, PMID: 16582911
- Viant C**, Fenis A, Chicanne G, Payrastré B, Ugolini S, Vivier E. 2014. SHP-1-mediated inhibitory signals promote responsiveness and anti-tumour functions of natural killer cells. *Nature Communications* **5**:5108. DOI: <https://doi.org/10.1038/ncomms6108>, PMID: 25355530
- Vyas YM**, Mehta KM, Morgan M, Maniar H, Butros L, Jung S, Burkhardt JK, Dupont B. 2001. Spatial organization of signal transduction molecules in the NK cell immune synapses during MHC class I-regulated noncytolytic and cytolytic interactions. *Journal of Immunology (Baltimore, Md)* **167**:4358–4367. DOI: <https://doi.org/10.4049/jimmunol.167.8.4358>, PMID: 11591760
- Vyas YM**, Maniar H, Dupont B. 2002a. Cutting edge: differential segregation of the SRC homology 2-containing protein tyrosine phosphatase-1 within the early NK cell immune synapse distinguishes noncytolytic from cytolytic interactions. *Journal of Immunology (Baltimore, Md)* **168**:3150–3154. DOI: <https://doi.org/10.4049/jimmunol.168.7.3150>, PMID: 11907066
- Vyas YM**, Maniar H, Dupont B. 2002b. Visualization of signaling pathways and cortical cytoskeleton in cytolytic and noncytolytic natural killer cell immune synapses. *Immunological Reviews* **189**:161–178. DOI: <https://doi.org/10.1034/j.1600-065x.2002.18914.x>, PMID: 12445273

- Wagtman N**, Rajagopalan S, Winter CC, Peruzzi M, Long EO. 1995. Killer cell inhibitory receptors specific for HLA-C and HLA-B identified by direct binding and by functional transfer. *Immunity* **3**:801–809. DOI: [https://doi.org/10.1016/1074-7613\(95\)90069-1](https://doi.org/10.1016/1074-7613(95)90069-1), PMID: 8777725
- Wang W**, Liu L, Song X, Mo Y, Komma C, Bellamy HD, Zhao ZJ, Zhou GW. 2011. Crystal structure of human protein tyrosine phosphatase SHP-1 in the open conformation. *Journal of Cellular Biochemistry* **112**:2062–2071. DOI: <https://doi.org/10.1002/jcb.23125>, PMID: 21465528
- Wang X-D**, Gong Y, Chen Z-L, Gong B-N, Xie J-J, Zhong C-Q, Wang Q-L, Diao L-H, Xu A, Han J, Altman A, Li Y. 2015. TCR-induced sumoylation of the kinase PKC- $\theta$  controls T cell synapse organization and T cell activation. *Nature Immunology* **16**:1195–1203. DOI: <https://doi.org/10.1038/ni.3259>, PMID: 26390157
- Watanabe N**, Gavrieli M, Sedy JR, Yang J, Fallarino F, Loftin SK, Hurchla MA, Zimmerman N, Sim J, Zang X, Murphy TL, Russell JH, Allison JP, Murphy KM. 2003. BTLA is a lymphocyte inhibitory receptor with similarities to CTLA-4 and PD-1. *Nature Immunology* **4**:670–679. DOI: <https://doi.org/10.1038/ni944>, PMID: 12796776
- Wu C**, Guan Q, Wang Y, Zhao ZJ, Zhou GW. 2003. SHP-1 suppresses cancer cell growth by promoting degradation of JAK kinases. *Journal of Cellular Biochemistry* **90**:1026–1037. DOI: <https://doi.org/10.1002/jcb.10727>, PMID: 14624462
- Wu Z**, Park S, Lau CM, Zhong Y, Sheppard S, Sun JC, Das J, Altan-Bonnet G, Hsu KC. 2021. Dynamic variability in SHP-1 abundance determines natural killer cell responsiveness. *Science Signaling* **14**:eabe5380. DOI: <https://doi.org/10.1126/scisignal.abe5380>, PMID: 34752140
- Zhou X**, Zhao R, Schwarz K, Mangeat M, Schwarz EC, Hamed M, Bogeski I, Helms V, Rieger H, Qu B. 2017. Bystander cells enhance NK cytotoxic efficiency by reducing search time. *Scientific Reports* **7**:44357. DOI: <https://doi.org/10.1038/srep44357>, PMID: 28287155